J. Webster (ed.), *Wiley Encyclopedia of Electrical and Electronics Engineering*

SUPERCONDUCTORS: PROCESSING OF HIGH-T_C BULK, THIN FILM, AND WIRES

Superconductors are a class of materials possessing two unique properties: the complete loss of electrical resistivity below a transition temperature called the critical temperature (T_c) and the expulsion of magnetic flux from the bulk of a sample (diamagnetism) in the superconducting state. The latter property is also known as the Meissner–Ochsenfeld effect or more commonly, the Meissner effect (1). At temperatures above T_c, these materials possess electrical resistivity like ordinary conductors, although their normal state properties are unusual in many aspects. The abrupt change from normal conductivity to superconductivity occurs at a thermodynamic phase transition determined not only by the temperature but also by the magnetic field at the surface of the material and by the current carried by the material. Several metals and metallic alloys exhibit superconductivity at temperatures below 22 K, and will be henceforth called low temperature superconductors (LTS). In 1950, superconductivity was explained as a quantum mechanical phenomenon by the London phenomenological theory (2). Later, the two-fluid phenomenological model explained the electronic structure of a superconductor as a mixture of superconducting and normal electrons, with the proportion of superconducting electrons ranging from zero at the onset of superconductivity to 100% at 0 K (3). In 1955, Bardeen, Cooper, and Schrieffer's (*BCS*) theory explained that superconductivity was the result of the formation of electron pairs of opposite spins (known as Cooper pairs), primarily owing to electron–phonon coupling (4). The BCS theory proved to be the most complete theory for explaining the superconducting state and the normal state of LTS materials. A major development in superconductors was the discovery by Josephson in 1963 that Cooper pairs show macroscopic phase coherence, and that such pairs can tunnel through a thin insulating layer sandwiched between two superconducting layers [the superconductor–Insulator–super-conductor (*SIS*) junction known as the Josephson junction] (5). This effect, called the Josephson effect (5), caused a flurry of activity in the fields of high-speed computer logic and memory circuits in the 1960s and 1970s, since it can be used to make high-speed low-power switching devices. Problems were encountered in the mass fabrication of Josephson junctions for complex systems such as digital computers. Although the applications of LTS for electrical applications and electronics were demonstrated, the cost of cooling was too high for the commercial development of LTS.

The era of high-temperature superconductors (*HTS*) began in 1986 when two IBM Zurich researchers, K. A. Muller and J. G. Bednorz, reported the occurrence of superconductivity in a lanthanum barium copper oxide (LaBaCuO) at 30 K(6). Soon after, M. K. Wu, P. W. Chu, and their collaborators at the University of Alabama and University of Houston (7), respectively, announced the discovery of 90 K superconductivity. Since these two historic discoveries, there has been substantial progress in HTS technology. Several new families of cuprates including BiSrCaCuO (8), TlCaBaCuO (9), and HgCaBaCuO (10) have been found to be superconducting above 90 K. These discoveries make feasible electrical and electronics applications at temperatures above the boiling point of liquid nitrogen (77 K). Cuprate superconductors with a T_c value higher than 30 K have been classified as high-temperature superconductors. The obvious advantage of using liquid nitrogen rather than liquid helium for cooling is its higher heat of vaporization, which not only simplifies the design of cryostats but also the cost of cooling. Furthermore, liquid nitrogen (at $0.25/liter) is more than an order of magnitude cheaper than liquid helium (at $5/liter). Progress made in cryocoolers has made feasible HTS applications in electrical wires,

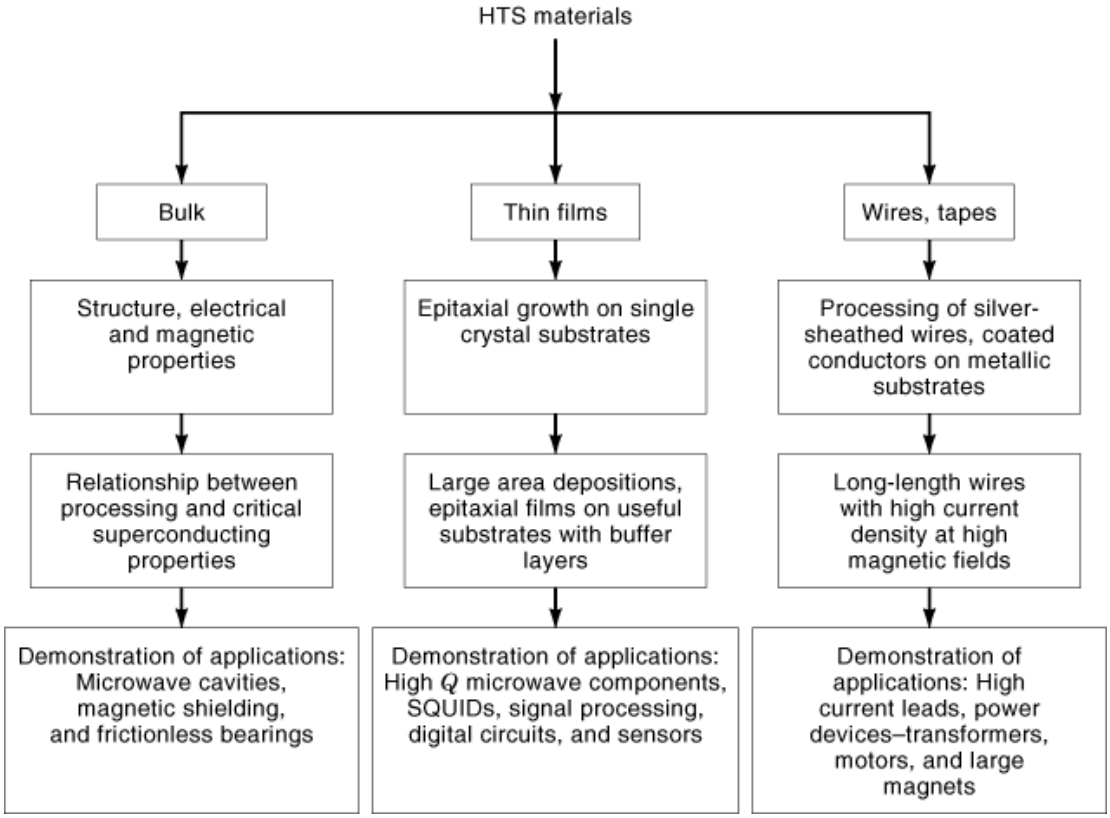

Fig. 1. A generalized road map for the HTSs technology. YBCO 123 compound has been the most studied material among the HTSs. Most applications have been demonstrated with the YBCO superconductor. Most applications in HTS wires have been demonstrated using BSCCO.

magnets, and electronics. The excitement and challenges posed by these HTS materials have touched multiple disciplines, such as physics, chemistry, material science, and electrical engineering. Tremendous progress has been made in the application of HTS materials in such areas as Superconducting Quantum Interference Devices (*SQUID*s), passive microwave devices, and long-length wires, as illustrated in the road map for the HTS technology, shown in Fig. 1. Better-quality materials emerging from refined processing methods have made it possible to separate the intrinsic properties of HTS from its extrinsic properties. The interrelationships of processing with structural, physical, electrical, and magnetic properties continues to be an area of intensive scientific research. In this article, we provide an overview of important high-temperature superconducting materials, their properties, and promising procedures for synthesizing bulk, thin film and wire forms of HTS conductors for engineering applications.

Properties of High-Temperature Superconductors

Magnetic Properties. The critical temperature (T_c) is defined as the temperature below which a superconductor possesses no dc electrical resistivity or the temperature below which a superconductor exhibits diamagnetic behavior. The useful range of operation of a superconductor is typically below 0.6 T_c, as other

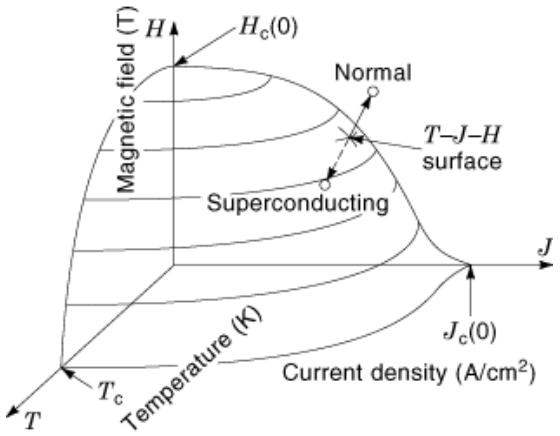

Fig. 2. Temperature–current–magnetic field (*T*–*J*–*H*) three-dimensional surface defining the operating limits for a superconductor.

important superconducting properties are enhanced below this temperature. Critical current density (J_c) is one of the most important superconducting properties for engineering applications. It is an estimate of maximum current density (current per cross-sectional area of the conductor) a superconductor can support before becoming a normal conductor. The critical field (H_c) for a superconductor is the maximum magnetic field below which a superconductor exhibits diamagnetic behavior and above which the superconductivity is quenched. The T_c, H_c, and J_c parameters define a point in three-dimensional space, and for superconductors these points span a volume as shown in Fig. 2.T_c, H_c, and J_c values are relatively low in type I superconductors. Type II superconductors are generally suitable for most electrical and electronic applications because of higher T_c, H_c and J_c values (11). In type I superconductors, the flow of shielding current in the superconductor is restricted to a thin layer from the surface, called the penetration depth (λ), when the magnetic field is below H_c. The penetration depth is very small near 0 K, and increases dramatically as the temperature approaches T_c. The penetration depth at 0 K ranges from 100 Å to 1500 Å for type I materials (11). Above the critical field, the magnetic field completely penetrates a type I superconductor, quenching superconductivity, as shown in Fig. 3. Figure 3 also illustrates the T-dependence of resistivity in a superconductor at $T > T_c$.

In type II superconductors,H_{c1} represents the lower critical field above which magnetic flux penetrates a superconductor to form a mixed state in which superconducting and normal electrons coexist. When $H > H_{c2}$, the upper critical field, superconductivity is largely confined to the surface of the material. In the mixed state, magnetic flux penetrates through small tubular regions on the order of the coherence length (ξ) (a length scale that characterizes superconducting electron pair coupling), called vortices (or flux tubes), with each vortex containing one quantum of flux, ϕ_0 (12). Abrikosov, in his study of type II superconductors determined that $\phi_0 = h/2e$, where h is Planck's constant and e is the electronic charge (12). The vortices form a periodic lattice called the Abrikosov vortex lattice. The resistivity of a superconductor may be vanishing in the mixed state, provided the vortices are pinned or trapped. As the applied magnetic field (H_a) approaches H_{c2}, the number of vortices increases until there can no longer be any more addition of vortices, at which point the material becomes a normal conductor. Figure 4 shows the magnetic properties of type II superconductors. In the mixed state, each vortex resides in a normal region, which is separated by superconducting regions. The vortices experience three different types of forces: one is the Lorentz force due to the flow of external current, experienced in the direction of and proportional to the vector product of the current and the vortex field. Second is the force of repulsion from other vortices, and third is the pinning force from metallurgical defects. The Lorentz force causes motion of vortices (also called the flux flow). The vortex motion produces an opposing electric field to the flow of current,

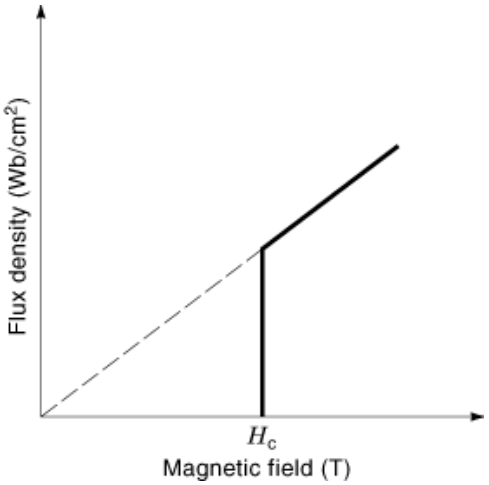

Fig. 3. A type I superconductor's magnetic flux density versus applied magnetic field. A type I superconductor will not have any flux enclosed in the bulk below the critical temperature. Above the critical field, the applied field completely permeates in the bulk of the material.

essentially contributing to ohmic losses. However, vortices can become trapped or pinned (called flux pinning) at metallurgical defects, in secondary phases or at impurity sites. Owing to the repulsive forces between each vortex, pinning a few vortices may lead to a frozen vortex lattice, or a lossless state, true only for direct currents and low-frequency alternating currents. The frozen vortex lattice occurs only below a critical field called the irreversibility field (H_{irr}). Some of the trapped vortices could remain in the superconductor, contributing to a hysteretic behavior when an alternating current is applied, which produces further dissipation of energy. The trapped flux is analogous to remanent flux in ferromagnetic materials. While pinning centers tend to prevent the movement of vortices, there is a tendency for vortices to jump over the pinning defects. This phenomenon is called flux creep. At $H_a > H_{irr}$, vortices will move, causing additional energy dissipation. Resistive transitions in a superconducting sample in applied magnetic fields are shown in Fig. 5. Transitions at higher fields clearly show additional ohmic losses (13). Although the upper critical field is generally higher in type II materials, the limiting field is the irreversibility field, which is an order of magnitude lower than H_{c2}. Owing to the complex nature of the cuprate ceramic superconductors, and operation at higher temperatures, the ac losses in HTS materials are generally higher than in LTS materials (14,15).

Structural Properties. The presence of one or more copper oxide (CuO2) planes in the unit cell is a common feature of all HTS materials, also referred as cuprate superconductors. The most popular cuprate materials are $Y_1Ba_2Cu_3O\ \delta$ (henceforth referred to as YBCO), $Bi_2Sr_2Ca_{n-1}Cu_nO_{2n+4}$ (where $n = 2, 3$) BSCCO (henceforth referred to as Bi2212, Bi2223 for $n = 2$, and $n = 3$, respectively), $Tl_2Ba_2Ca_{m-1}Cu_mO_{2m+4}$ (henceforth referred to as Tl2201, Tl2212, and Tl2223), and $HgBa_2Ca_{m-1}Cu_mO_{2m+2}$ (where $m = 1, 2, 3$). Table 1. lists the well developed cuprate superconductors, their superconducting properties, and important applications demonstrated to date. In YBCO, there are two square planar CuO_2 planes stacked in the c-direction, separated by an intercalating layer of barium and copper atoms and a variable number of oxygen atoms. The conventional wisdom is that the CuO_2 planes are the conduction channels of superconductivity, whereas the intercalating layers provide carriers or act as charge reservoirs necessary for superconductivity, although this view is not shared universally (16). The charge density, the number of superconducting charge carriers per unit volume, is determined by the overall chemistry of the system and by the charge transfer between the CuO_2 planes and the CuO chains. The charge density in a HTS material (10^{19}/cm^3) is two orders of magnitude lower than conventional LTS (10^{21}/cm^3). Remarkably, the oxygen content in the system changes the oxidation

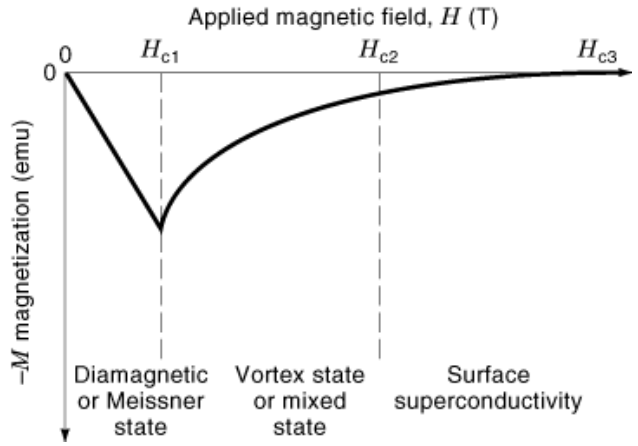

Fig. 4. The magnetic behavior of a type II superconductor, showing the Meissner state behavior below H_{c1}, mixed state behavior between H_{c1} and H_{c2}, and the surface superconductivity between H_{c2} and H_{c3}.

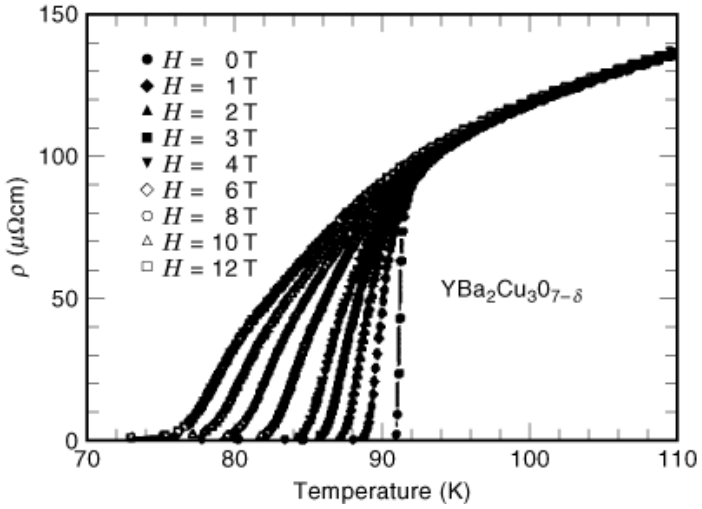

Fig. 5. Temperature dependence of resistivity for an epitaxial c-axis-oriented YBCO thin film at different magnetic fields, with the field parallel to the c-axis. Courtesy of 13.

states of the copper chain atoms, which, in turn, affects their ability for charge transfer, charge density, and superconducting properties. Depending on the oxygen content, the YBCO 123 material could have a nonsuperconducting tetragonal ($a = b \neq c$) phase or a 90 K superconducting orthorhombic ($a \neq b \neq c$) phase. When fully oxygenated, YBCO possesses an orthorhombic unit cell with typical dimensions of $a = 3.85$ Å, $b = 3.88$ Å, and $c = 12.0$ Å, and a $T_c = 90$ K. Figure 6 shows the crystal structure of YBCO 123 and BSCCO 2223 superconductors, showing the conduction layers and the binding layers in each case.

BSCCO superconductor contains a weakly bonded double BiO layer that separates the CuO_2 planes. The Bi2223 structure is part of a family of several other HTS compounds in which Bi is replaced by Tl or Hg (with different oxygen coordination) and partially by lead. In some cases, the double layer of these metal-oxide layers can be reduced to a single layer-yielding another family of superconductors such as 1212 or 1223 [e.g.,

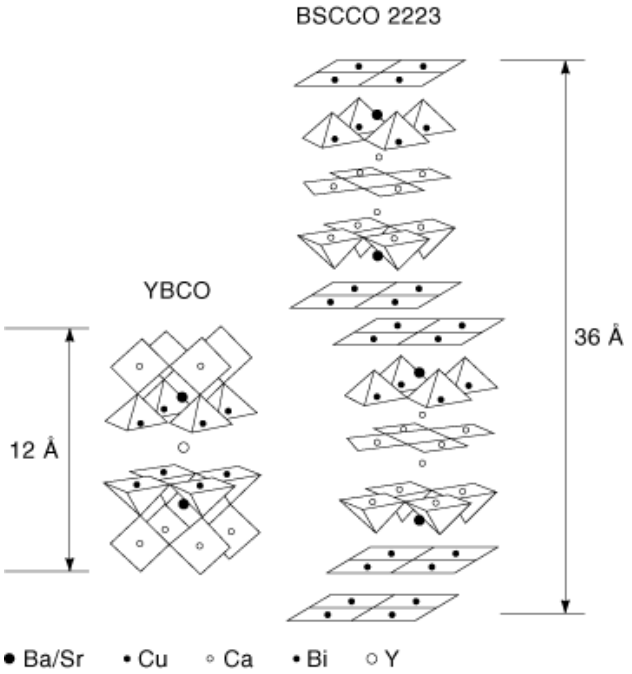

Fig. 6. The crystal structure of YBCO 123 and BSCCO 2223 compounds, showing the conducting layers, and the binding layers.

Table 1. Promising HTS Materials, Properties, and Applications

Material	T_c	$J_c(0)$ and $J_c(H)$ (A/cm^2)	Applications
Bulk $YBa_2CU_2O_{7-\delta}$ (123) YBCO (melt grown)	90 K	10^5 at 77 K ZF 10^4 at 77 K 10T	HTS cavities Bearings, EM shield
Thin-film YBCO on crystalline substrates	90 K	10^7 at 77 K ZF 10^6 at 77 K 5T	SQUIDs, microwave Electronics
$Tl_2Ba_2CaCu_2O_8$ (2212) thin film	97–100 K	2×10^6 at 77 K ZF 1×10^5 at 77 K 0.1T	Microwave Electronics
$Tl_1Ba_2Ca_2Cu_3O_{10}$ (1223) thin film	117–123 K	2×10^6 at 77 K ZF 5×10^4 at 77 K 1T	Microwave Electronics
$Bi_2SrCa_2Cu_2O_8$ wires/tapes	90 K	10^4 at 77 K ZF 10^3 at 77 K 1T 10^5 at 4 K ZF 10^4 at 4 K 1T	Low-field HTS wires for 20–30 K applications
$Bi_2Sr_2Ca_2Cu_3O_{10}$ wires/tapes	110 K	$5–7 \times 10^4$ at 77 K ZF 5×10^3 at 77 K 1T	Magnets, current leads, SMES

$(Tl–Pb)_1Ba_2Ca_2Cu_3O_{10}$ henceforth is referred as Tl1223]. The single-layer compounds offer strong flux pinning and low intrinsic defect structure compared to the double-layer compounds. The presence of a weakly bonded BiO layer is crucial for their superconducting properties in the Bi2212 and 2223 systems. The mechanical properties of Bi2212 and 2223 are micaceous, (mica-or clay-like), and they have highly anisotropic growth rates along the ab- plane and c-direction. The latter is important to process long-length wires and to enhance

the electromagnetic connectivity of the grains, thus making high transport current densities over long lengths possible (17). This is mainly due to the weak interlayer bonding of the BiO layer with the CuO_2 planes. On the other hand, the weak interlayer bonding of the BiO layer also leads to intermixing of Bi2212 and Bi2223 phases. In spite of this weakness, better grain connectivity and micaceous crystalline morphology are attractive for developing long-length HTS wires. Tl2212 and 2223 compounds have a structure similar to the Bi2212 and 2223 compounds with (TlO) double layers replacing the BiO layers.

Other Important Properties. All the popular HTS materials possess a fundamental limitation, crystalline anisotropy, (i.e., they possess different structural and electrical properties in different directions). Superconducting properties such as critical current density (J_c) and critical magnetic field (H_c) along the ab-planes (xy) are superior to those along the c-axis (z). A major challenge for researchers has been to develop textured samples to take advantage of high J_c in the ab-planes. The HTS materials also exhibit higher penetration depths compared with LTS materials. The penetration depth is an important parameter for high-frequency applications of superconductors. It is defined as the depth through which a magnetic field penetrates into a superconducting sample and decays to $1/e$ of the field at the surface. The magnetic field decays in the form of $H = H_0 e^{-x/\lambda}$, where H_0 is the field at the surface,x is the depth through the sample, and λ is the penetration depth of the superconductor, analogous to the skin depth in conventional electrical conductors. Penetration depthλ (T) increases with temperature. Penetration depth is a frequency independent parameter in contrast to the frequency-dependent skin-depth of normal conductors. This means that little or no dispersion will be introduced in superconducting components, and that it will be negligible up to frequencies as high as tens of gigahertz, in contrast to dispersion present in normal metals. Furthermore, lower losses in superconductors lead to a reduction in physical size, and this feature represents another advantage for HTS thin-film based circuits. Compact delay lines, filters, and resonators are possible with a high-quality factor (Q) due to low-conductor losses (see Superconducting filters and passive components). The challenge in processing involves developing HTS materials with smooth-surface morphology to minimize high-frequency ac conductor losses. The extremely short coherence length in HTS materials ($<$30 Å along the ab-plane) increases the difficulty of making Josephson junctions (see (Tunneling and josephson junctions).

Processing of High-Temperature Superconductors

Although T_c and H_c values of a superconductor are generally intrinsic properties of a specific material,J_c and λ values, on the other hand, are a function of sample microstructure and can vary by several orders of magnitude owing to various processing techniques. A high J_c in large magnetic fields is desirable for electrical applications of HTS. In general, J_c greater than 10^5 A/cm^2 at 77 K is required for wires, tapes, and magnets for high magnetic field applications (17). Although high J_cs in HTS are achieved in bulk, thin films, and wires, several processing-related problems need to be addressed. These problems relate to grain boundaries, metallurgical defects, flux pinning mechanisms, and flux creep. Grain boundaries are interfacial regions between adjacent grains and could contain impurity phases, normally conducting or insulating, extending beyond the coherence length of these superconductors. These grain boundaries create superconductor–normal conductor or insulator–superconductor Josephson junctions, the critical currents of which are much lower than in a homogenous superconductor, and hence they are called as weak links. The grain boundaries are particularly a problem in polycrystalline bulk superconductors because they affect the bulk critical current density. Grain boundaries also contribute to surface resistance of a superconductor at high frequencies because they increase the residual ac losses. Processing of HTS materials to improve J_c requires ways to minimize the grain-boundary effects and enhance the flux pinning sites in the superconductors. Addition of a small percentage of silver into HTS materials improves the critical currents of grain boundaries. Also, texturing of a bulk superconductor to align grains along ab-planes reduces the detrimental effects of grain boundaries. It has been determined that the presence of low-angle grain boundaries [i.e., adjacent grains interfacing at a low angle ($\leq 10^\circ$)], is not

deleterious to J_c (18). However, the elimination of high-angle grain boundaries in HTS materials has been a difficult challenge to overcome. Recent developments in YBCO-coated conductors show promise in reducing the presence of high-angle grain boundaries, discussed later. To date, YBCO is the most successful candidate for enhancements in flux pinning (19). Enhancement of flux pinning and suppression of flux creep have been achieved by the introduction of controlled amounts of defects, such as co-existing normal secondary phases by alloying, or by neutron or proton irradiation to define normal regions along the particle trajectory that give rise to higher J_c s and higher H_cs (20).

Tremendous progress has been made in the synthesis of bulk single-phase HTS conductors, silver-sheathed wires, tapes, and thin-film-coated conductors in the past decade as shown in Table 1.. Bulk conductors with large volume fraction of superconductivity are being routinely synthesized in YBCO-, Tl-, and Bi-based HTS materials. Improved powder synthesis, understanding of reaction chemistry, and phase diagrams have led to increased phase purity and improved flux pinning (resulting in higher current density at self field). Solid-state reaction and melt texturing are the two widely used processing methods for bulk HTS.

Processing of Bulk Superconductors

There are three important process considerations for the choice of bulk superconductors for applications such as magnets, current leads, and superconductor magnetic energy storage systems (1) growth of large-area, single-phase bulk conductors, (2) ease of introducing strong flux pinning centers in the bulk, to enhance the critical currents, and (3) long-term stability, (i.e., ability to withstand thermal cycling to modest temperatures) and aging under ambient conditions. Among the various bulk superconductors, YBCO appears to be the most plausible for electrical applications since the details of the crystal structure have been reliably established, and it is easy to synthesize single-phase specimens. Moreover, in YBCO, introduction of flux pinning centers to enhance J_c has been demonstrated, although this is not the case in Bi, Tl, and Hg superconductors. Further, melt-processing growth of YBCO superconductors provides grain-alignment resulting in J_c as high as 10^5 A/cm^2 at self field and 77 K (21). In the case of YBCO, the melt-powder-melt growth (*MPMG*) processing has significantly improved performance of bulk materials. The thallates are also attractive as T_c as high as 125 K, J_c in bulk greater than 10^5 A/cm^2 at 77 K and zero field (22) have been achieved. An advantage with the thallates is that multiple phases, especially Tl2223 and Tl2212 phases, can coexist, without degrading the superconducting properties in bulk conductors, thin films, and wires. The magnetic field dependence of J_c is comparable to the best YBCO superconductors. A disadvantage of thallates is the toxicity of Tl, which needs very careful handling and processing. The volatility of Tl gives rise to its losses during high-temperature synthesis. Most of the thallates contain structural defects, which affect the superconducting properties negatively. The thermodynamics of Tl-based compounds is quite different from other HTS materials due to the volatility of Tl (23).

At the present time, the synthesis of mercury-based HTS has unique problems mainly due to the volatility of mercury compounds. Since HgO decomposes around 500°C, all processing must be done in a sealed environment in the production of bulk superconductors. Also, the Bi compounds are not attractive for bulk conductors primarily due to the polycrystalline nature of the grains and weak flux pinning above 30 K (19). Melt-texturing Bi compounds is not as simple as the YBCO. Bismuth compounds are generally thought to be attractive for wire applications owing to their micaceous morphology. In the following section, we provide processing details on YBCO, Tl2212, and Tl1223 bulk superconductors.

Processing YBCO 123 Bulk Superconductors.

Conventional Solid-State Reaction Method. The conventional means of producing bulk HTS materials is the solid-state reaction method, or calcination. Carbonates, or oxides of Ba, Ca, Cu, and Y as starting materials, are mixed and ground to the desired size and then heat-treated in an alumina crucible at temperatures as high as 950°C for 24 h. After cooling to room temperature, the reacted sample is finely ground and mixed

again and heat-treated for an additional 24 h; this step is repeated to promote homogeneity. The samples are then pelletized in desired shapes using a hydraulic press at a typical pressure of 1500 psi. The pellets are placed in a crucible made of gold or platinum or alumina, introduced into a furnace preheated to 900°C, and sintered typically in air for 24 h. Oxygen is introduced into the furnace at around 500°C, during slow cooling of the samples to room temperature. This gives rise to the growth of the orthorhombic superconducting phase. Although the technique is fast, there are undesirable phases present in samples prepared this way, typically $BaCuO_2$, CuO, and possibly some contamination from the heat-treatment process. In spite of these limitations, it is possible to get T_c of 90 K and current densities of 10^4 A/cm^2 at zero field at 77 K. The polycrystalline nature of grains in such samples results in poor field dependence of J_c, with J_c decreasing by three orders of magnitude in a magnetic field of 0.1 T.

Texturing of YBaCuO 123 Superconductors. Texturing of YBCO can be achieved using mechanical, magnetic, and melt-growth techniques. The mechanical and magnetic means produce only a marginal improvement in superconducting properties, mainly owing to the presence of large-angle grain boundaries, whereas melt growth techniques reduce the large-angle grain boundaries and improve the critical currents significantly. The melt-texturing techniques are the most suitable for enhancement of J_c. Among the melt-texturing methods, melt texture growth (*MTG*) (21), quench and melt growth (*QMG*) (24), and melt powder melt growth (21) are techniques developed for nondirectional solidification. In these techniques, large YBCO crystals grow stacked along the *c*-axis, with improved connectivity between grains. Directional solidification is also possible by providing the right thermal gradient during the melt processing, either by the movement of the furnace or the sample. Directional solidification methods align the grains along the *ab*-planes, the direction of current flow, thus improving the current-carrying capability. It is also possible to align the grains along a preferred orientation using seeded melt growth (25) and liquid phase removal methods (26). In the seeded melt growth technique, a directionally oriented single crystal Sm123 or Nd 123 is used as a seed material to grow YBCO, oriented along the same preferred direction.

The melt texture growth of YBCO 123 involves melting the YBCO above its peritectic temperature, approximately 1010°C, in air. When heated above this temperature, the 123 compound undergoes incongruent melting to form a solid and a liquid phase according to the following reactions (27)

$$\begin{aligned} &YBa_2Cu_3O_x \rightarrow 1010^\circ C < T < 1300^\circ C \rightarrow \\ &\quad Y_2BaCuO_5(211/\text{green phase}) + \text{Liquid phase} \\ &Y_2BaCuO_5(\text{green phase}) + \text{Liquid phase} \rightarrow \\ &\quad 1300^\circ C < T < 1500^\circ C \rightarrow Y_2O_3 + \text{Liquid} \end{aligned}$$

On subsequent slow cooling, large oriented domains of 123 phase with 211 (green phase) inclusions are formed. In such samples, grains grow preferentially along *ab*-planes, are stacked along the *c*-direction, and are coupled by low-angle grain boundaries. This microstructure is in contrast to small randomly oriented polycrystalline grains obtained by solid-state reaction. Quenching studies performed on MTG samples show the presence of faceted growth interfaces where the 211 volume fraction and particle size decrease abruptly upon being included into the growing 123 grains. The 211 phase appears to provide Y into the growing phase of 123. The MPMG process is the most commonly used melt growth process designed for smaller sizes of the 211 precipitates, and homogenous distribution of the precipitates. This technique involves reaction of Y_2O_3 with a liquid phase to form the 211 phase. The nonuniform distribution is handled by taking the powder and crushing and remixing the melt quenched samples. This powder is pressed into a pellet and subjected to the melt growth. It was found that the samples should not be held above the peritectic temperature for too long because the 211 phase will grow into coarse grains. After a short time above the peritectic temperature, it is cooled to just below the peritectic temperature and then slow-cooled in flowing oxygen to room temperature. The temperature profiles for MTG and MPMG processing techniques are shown in Fig. 7. The critical temperatures are identified for

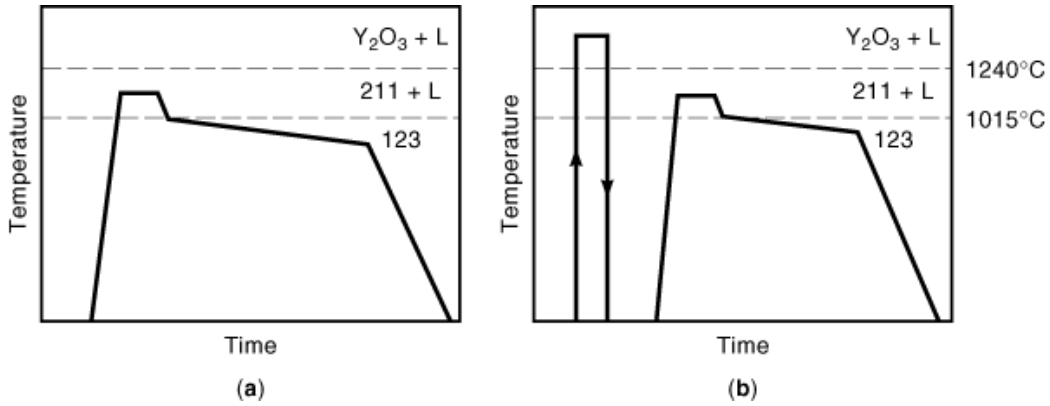

Fig. 7. Temperature profiles for (a) the melt texturing growth and (b) the melt process melt growth. Courtesy of 27.

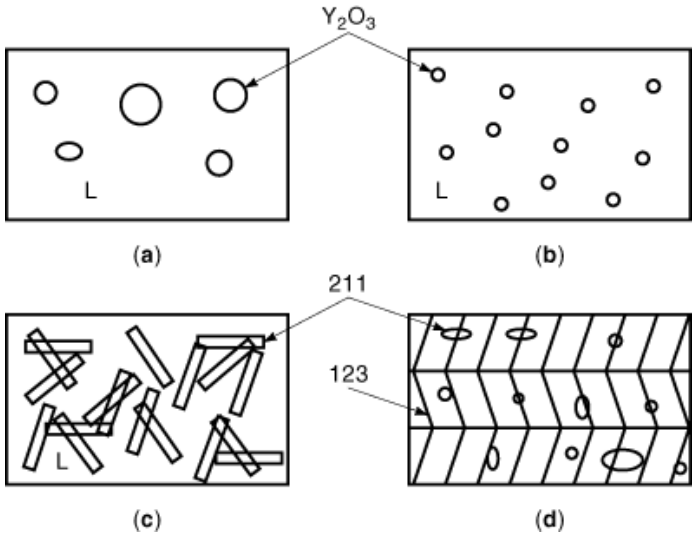

Fig. 8. Schematic representation of microstructure evolution in the MPMG growth of YBCO: (a) after quenching—yttria and solidified liquid; (b) during heating to the 211 + L region—yttria particles redesolving; (c) in the 211 + L region; and (d) final microstructure showing the 123 and 211 phases. Courtesy of 27.

both processes. The evolution of the microstructure during the MPMG process is shown in Fig. 8 (27). The figure illustrates the formation of 211 inclusions into the liquid phase.

The seeded melt growth is the most promising for large area domains of YBCO (27). In this technique, a single crystal seed of Sm123 or Nd123 is embedded in a presintered Y123 bar, and the whole assembly is introduced into a modified Bridgeman furnace for 15 min to 30 min and then withdrawn at a very slow rate of 1 mm/h. As the growth front of Y123 passes by the seed, seeded growth occurs at the interface. Because of the favorable alignment along *ab*-planes, large current densities, as high as 46,000 A/cm^2 at 77 K and zero field have been demonstrated. In the melt growth techniques, the hold time and cooling rate have a strong influence on the microstructure of the samples, determining the grain size and nature of the grain boundaries. The hold time determines the amount of liquid phase formed for the peritectic recombination. The cooling rate determines the time available for the recombination of the liquid (25).

Processing of TBCCO 2212 and 1223 Superconductors. In general, processing of thallates with high superconducting volume fraction (V_{sc}) has been difficult, primarily because of the volatility of Tl. Processing of Tl based HTS can be done either using an open system, or a closed system. In the open system, a sample is heat treated in an oxygen atmosphere or air at temperatures between 850°C and 900°C, for 10 min to 15 min. In a closed system, samples are sealed in a gold tube and heat-treated for longer times of 24 h to 48 h (28). The open system is susceptible to loss of Tl and, hence, requires additional compensation for Tl. The closed system has the disadvantage of sealing the samples in a container or a foil, resulting in reaction between the Tl-based compound and the container. In our work, we were able to synthesize samples with T_cs greater than 100 K for the Tl2212 phase and 115 K for the Tl1223 phase, with superconducting volume fractions greater than 50% in each case, by tuning the process parameters (29). The processing parameters that were optimized included the starting compositions of the compounds, sintering temperatures, and sintering times. The starting compositions are critical mainly because of the loss of Tl during heat treatments. In the 1223 superconductor the Hitachi composition of $Tl_{0.5}Pb_{0.5}Sr_{1.6}Ba_{0.4}Ca_2Cu_3O_y$ has been a popular starting composition for high-quality 1223 superconductor (30). In our study, we examined the role of different Ba concentrations and excess Tl and Pb doping concentrations to obtain a single phase 1223 superconductor in an open system (29).

Tl2212 samples were synthesized starting from $BaCuO_2$, CaO (99.999%) and Tl_2O_3 (99.999%) compounds. $BaCuO_2$ was prepared by mixing BaO_2 (99%) and CuO (99.99%) in equal molar portions and heat treating at 900°C for 24 h in air. The latter step was repeated after regrinding the pellet to promote homogeneity. $BaCuO_2$, CaO, and Tl_2O_3 were mixed in a molar ratio of 2:1:1.07, pelletized, and reacted in an enclosed Pt crucible. Our results indicate that samples sintered at 850°C for 10 min followed by a second heat treatment at 860°C for 10 min displayed optimum superconducting properties, which included a sharp T_c of 97 K, with a superconducting volume fraction as high as 54%. The porosity of the samples appears to be the limiting factor for the V_{sc}.

The first step performed in the synthesis of (Tl,Pb)(Sr, Ba) CaCuO 1223 superconductor, was the preparation of a SrCa CuO precursor, starting from 99.999% pure CaO and CuO and 99% pure SrO. Appropriate molar portions of SrO, CaO, and CuO were mixed, heated to 900°C for 24 h, cooled, and ground into a fine powder; then the same process was repeated to obtain a homogeneous precursor compound. For the Ba-doped samples, appropriate amounts of 99.99% pure BaO_2 were alloyed with SrO, in the precursor. The second step was to add appropriate amounts of 99.999% pure PbO and Tl_2O_3 to the precursor. Pellets of approximately 500 mg were made and heat-treated in an enclosed Pt crucible, at a temperature of 870°C for 10 min, followed by a slow cooling.

Characterization of Bulk Superconductors

Structural Characterization. The primary characterization of any form of a superconductor consists in establishing the structure by X-ray diffraction (*XRD*). Xrays from a source are collimated to strike the sample at an incident angle and Bragg scattered from the sample. For X rays, atomic planes of the material serve as a diffraction grating, causing the monochromatic X-ray beam to diffract and form a pattern. From an XRD pattern, one can establish the various phases populated and, in principle, the crystal structure including lattice parameters of each phase. In practice, since the *c*-axis lattice parameter depends on the oxygen content, XRD patterns can be used effectively to correlate structural results with superconducting parameters. If there is more than one phase present in a sample, the XRD patterns can be used to obtain quantitatively the concentration of various phases present in a sample. Since bulk materials synthesized by solid-state reaction are polycrystalline, the XRD pattern from such a sample has peaks corresponding to scattering from different crystallographic planes such as (100), (110), and (001). Powder XRD is an effective means to establish the major phases present in a sample.

Magnetic Properties. Vibrating sample magnetometer (*VSM*) is a widely used technique for the study of all types of magnetic materials as it permits a measurement of the dc magnetization of a sample. In HTS materials, VSM permits establishing the T dependence of the diamagnetic susceptibility in both a zero-field-cooled (*ZFC*) and a field-cooled (*FC*) configuration. In the VSM technique, a sample is placed in a uniform magnetic field and vibrated at a low frequency so as to induce a voltage signal in a pickup coil proportional to the magnetic moment of the sample. The magnetic moment is proportional to the product of the sample susceptibility and the applied field (30). Measurements are typically performed at several temperatures to obtain the magnetic and superconducting properties. A plot of the magnetization versus applied magnetic field can yield the magnetization J_c using the Bean's critical state model. For a cylindrical sample, the magnetization J_c is approximately 30 $\Delta M/d$ where ΔM represents the width of the hysteresis loop at a particular applied field H, and d the effective thickness of the sample normal to the applied field (31). This model typically results in an overestimate of the actual J_c. A more direct method to determine the transport J_c is by using the four-point probe method, in which a 1 μ V/cm electric field criterion is used to establish the transport J_c. Other magnetization measurement techniques include ac and SQUID magnetometers. In the ac magnetometer, a sinusoidally oscillating field is used. The primary coil is surrounded by a set of oppositely wound detector coils. Introducing a magnetic sample into the center of one or the other secondary detector coil leads to a voltage imbalance in the secondary circuit (32). The resulting flux change leads to a measurable induced emf, which is proportional to the sample susceptibility. Magnetic moment sensitivities as low as 10^{-8} emu are possible using a commercial ac susceptometer. Enhanced sensitivity can be obtained using a SQUID magnetometer, as SQUIDs are used in the detector circuitry. There are a large number of tools available for researchers to correlate the physical properties with the processing variables. Table 2. lists characterization tools used by HTS researchers, the outcomes from each tool, and corresponding observable.

Structural, Electrical, and Magnetic Properties of Bulk Superconductors. YBCO (123) Superconductors

The T_c of YBCO is near 90 K, provided the oxygen content in YBCO is optimal. YBCO, in particular, has remarkable of T_c sensitivity to oxygen stoichiometry as displayed in Fig. 9 (33). Specifically, one finds that at $\delta = 7.0$ in the $Y_1Ba_2Cu_3O_\delta$ superconductor,$T_c = 90$ K. For $\delta < 6.2$, $T_c = 0$ K. The plot of Fig. 9 also reveals that in the range $6.6 < \delta < 6.8$, $T_c = 60$ K, and displays a plateau, a feature that is identified with the existence of a superstructure in oxygen bonding. Figure 9 also reveals that it is not only the value of δ, but also the distribution of oxygen in the structure that controls the value of T_c. For YBCO, it is well established from neutron Bragg diffraction measurements that oxygen in the CuO_2 planes remains intact, whereas oxygen in the chains (CuO_3) diffuses at modest temperatures $T > 300^\circ$C and effuses out of the structure at $T > 500^\circ$C. An orthorhombic to tetragonal phase transformation occurs near an oxygen content of $\delta = 6.5$. Oxygen can be reversibly desorbed and absorbed from YBCO either by heating in a vacuum or an oxygen ambient, respectively. Plasma oxidation has been demonstrated as an attractive means to oxygenate HTS at rather modest temperatures for microelectronic applications. At a local level, it appears that the $T_c(\delta)$ variation can be traced to the length of the Cu(1)–O(4) bond that displays a threshold behavior as shown in Fig. 10 (33). Superconductivity in YBCO commences when the Cu(1)–O(4) bond length acquires a value of 1.82 Å or larger. Bond lengths less than 1.82 Å, apparently couple the pyramidal oxygen O(4) to the Cu(1) chain cations, inhibiting charge transfer from the chains to the CuO_2 planes. Oxygenation of YBCO to a value of $\delta \approx 6.5$ gives a Cu(1)–O(4) bond length close to the threshold value.

The melt-textured samples have higher J_c compared with conventional solid-state-sintered samples. Figure 11 shows the enhanced J_c typical of melt-processed samples (14,15). For comparison,J_c of an epitaxial YBCO thin film is shown. The figure shows improvement in J_c for melt-textured samples compared with the conventionally sintered samples. Melt-processed samples have at least an order of magnitude higher in-field J_c and do not drop as rapidly at higher fields as the sintered samples.

2212 superconductors. Synthesis of the Tl2212 superconductors was performed by reacting appropriate amounts of the $Ba_2Ca_1Cu_2O_5$ precursor with Tl_2O_3. The results of three samples each processed differently

Table 2. Basic Materials Characterization Tools Used for Research in High-T_c Superconductors

Method	Observable	Outcomes
Four Point Probe, at 0 field and applied Magnetic field	T_c, Transport J_c	Resistivity above and below T_c, presence of flux creep
Dc magnetometer	Diamagnetic susceptibility, T_c magnetization J_c	Superconductong volume fraction
Ac magnetometer	T_c, real and imag.-susceptibility (χ and χ'')	Superconducting volume fraction, weak link dissipation
SQUID magnetometer	T_c, diamagnetic susceptibility, Josephson tunneling	High-resolution diamagnetic susceptibility, symmetry state of pairing wave functions
Microwave conductivity	Surface resistance	Penetration depth at 0 K, conductor losses
X-ray diffraction	Lattice parameters, symmetry	Crystal structure, presence of secondary phases, grain alignment
EXAFS	Local co-ordination of atoms	Local atomic scale structure, bonds
Mossbauer spectroscopy	δ, Δ local fields, f-factor	Chemically specific local structure; local vibrational density of states
Inelastic neutron scattering	$g(\omega)$: vibrational density	Total vibrational density of states
Raman scattering	Phonons and phonon line shapes	Isotope effect, electron phonon coupling
Electron energy loss spectroscopy (EELS)	Local chemistry	Oxygen hole distribution
Thermogravimetric analysis (TGA)	Sample weight loss	Oxygen stability
Calorimetry	Specific heat capacity	Nature of pairing state
Auger electron spectroscopy	Surface chemistry, electronic density of states	Electronic structure near the Fermi-level and origin of pairing

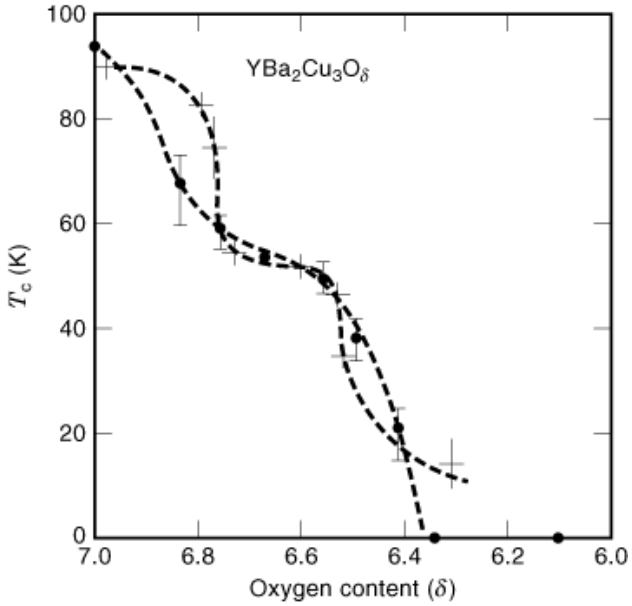

Fig. 9. Critical temperature versus oxygen content for YBCO samples. The dots and crosses were measured on samples with oxygen removed by high-temperature quenching and low-temperature gettering, respectively. Courtesy of 33.

are presented here. Sample 1.1 was processed at 850°C for 10 min. Sample 1.3 was processed at 850°C for 10 min followed by an additional heat treatment at 860°C for 10 min. Sample 1.6 was prepared by heat treatment at 850°C for 10 min followed by heat treatment at 860°C for 45 min. From XRD measurements, all samples showed the characteristic Bragg reflection peaks of the $Tl_2Ba_2CaCu_2O_8$ phase. No other impurity phases were detected in the XRD scans. Figure 12 shows the XRD reflections for the three samples in which characteristic peaks of the Tl2212 phase are clearly visible. Figure 13 shows the magnetization hysteresis loops of the three samples recorded at 15 K. The magnetization scale for all samples was normalized to their mass. As seen in Fig. 13, the diamagnetism displayed by sample 1.3 is the largest among the samples investigated. This result has been reproduced in several samples. Figure 14 displays the temperature dependence of magnetic susceptibility. In this figure, the scans are labeled according to the second heat-treatment temperature and time. One finds that the second-step heat treatment at 860°C for 10 min not only increases the saturation diamagnetization at $T = 15$ K but also significantly narrows the width of the superconducting transition, without affecting the T_c value. Our conclusion is that the second-step heat treatment produces more strain-free material, or chemical ordering of the phase. The underlying structural growth does not alter the bulk T_c, but do significantly enhances the diamagnetic response (Fig. 14), owing due to growth of a more strain-free material. The superconducting volume fractions for samples 1.1, 1.3, and 1.6 were 37%, 54%, and 27%, respectively. Clearly, the process conditions used for sample 1.3 appear to optimize growth of the superconducting phase. Further increase in the second-step heat treatment time, resulted in an increase of T_c to above 110 K. It has been shown by Sugise et al. (34), that prolonged heating of Tl2212 samples in air can grow bulk 2223 samples. Depletion of Tl_2O_3 from Tl2212 samples essentially leads to the transformation of the two-layered cuprate Tl2212 into the three-layered cuprate Tl2223 structure. Since the XRD scans provide no evidence of presence of the 2223 phase, it must be present as stacking faults, or planar defects, as documented by Raveau et al. (35) using high-resolution electron microscopy. Also, in Fig. 14, note that the sample with second-step 20 min heat treatment in a sealed gold tube displays much smaller diamagnetism than the samples heat-treated in a Pt

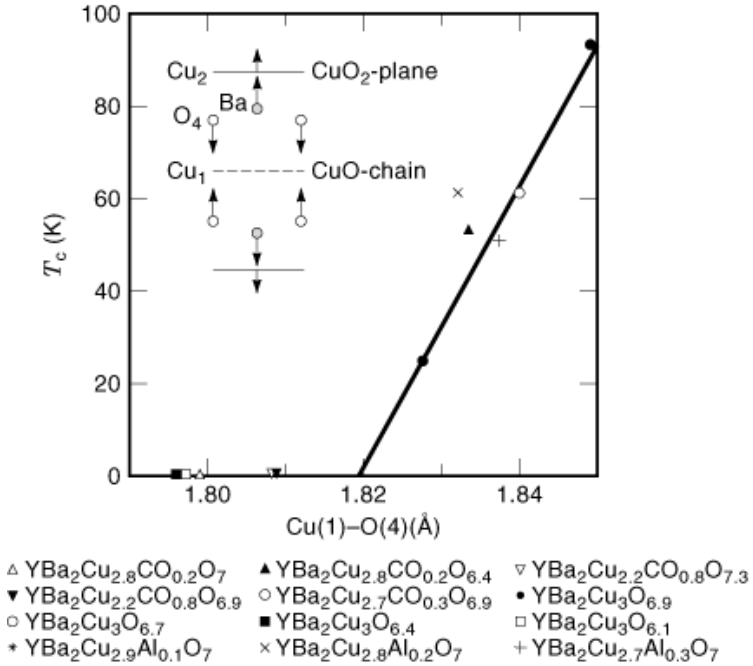

Fig. 10. Critical temperature versus Cu(1)–O(4) (copper in the chain bridging oxygen) bond length in the 123 phase. Also shown are data for dopants introduced into the YBCO phase, with similar structural changes. As shown in the inset, the CuO_2–CuO_2 plane distance increases, the O(4) moves toward the CuO chains, and the Ba moves toward the CuO_2 planes. Courtesy of 33 and references therein.

crucible. This is evidence of a reaction between the thallates and the gold tube at 860°C in a closed system and suggests that gold should be avoided as a crucible for processing in a closed system of thallate superconductors.

Tl1223 Superconductors. For the synthesis of 1223 compound, the starting composition of $Tl_{0.5}Pb_{0.5}Sr_2Ca_2Cu_3O_9$ (1223) stoichiometry upon thermal processing yielded samples with 1223 and 1212 phases that had a T_c of 107.5 K and a volume fraction of 55%. Replacement of some Sr by Ba in the starting composition $Tl_{0.5}Pb_{0.5}Sr_{2-x}Ba_xCa_2Cu_3O_9$, on the other hand, yielded samples that had the 1223 phase. Samples with a Ba content $x < 0.4$ clearly were found to have both 1212 and 1223 phases, whereas samples with $x > 0.4$ showed principally the 1223 superconductor. At $x = 0.75$, samples containing only the 1223 phase were obtained upon heat treatment at 870°C for 11 min, using starting materials in which 50% additional Tl_2O_3 and PbO were compensated. Low-field ac susceptibility measurement of the sample shown in Fig. 15 reveals an onset T_c of 117 K with a superconducting volume fraction of about 50%. Note that the in-phase susceptibility does not indicate the presence of minority phases. Samples with a Ba content of $x = 0.75$ showed the highest T_c of 117 K. Our results indicate that a minimum Ba content of $x = 0.4$ is necessary to produce a majority 1223 phase, which appears to be consistent with the Hitachi composition. Our study also demonstrates that the highest T_c, with the largest superconducting volume fraction are obtained at a Ba content of $x = 0.75$, in Tl and Pb over compensated samples.

Metal-Doping Effects in YBCO Bulk Superconductors. Doping transition metals of group III (Fe, Co, Ni) in YBCO exemplifies the trials and tribulations of working with high T_c superconductors. As material quality has improved, so have the challenges to understand the nature of the pairing state. One of the areas that has been intensively studied is the doping of Fe in YBCO. More than 1000 papers have been published

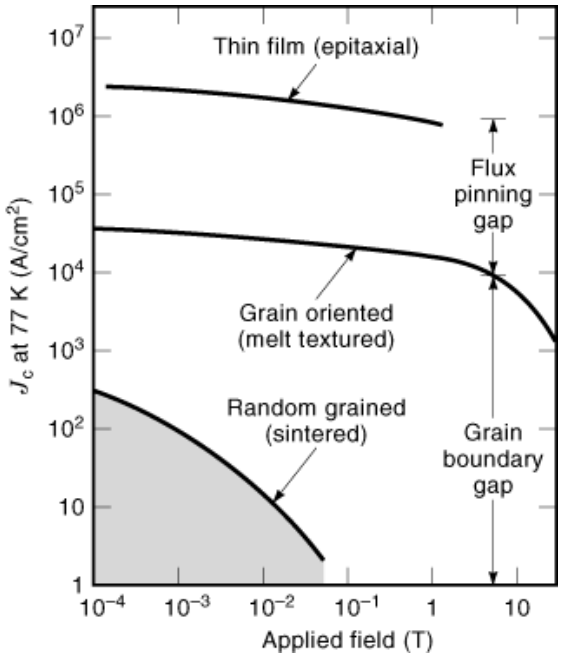

Fig. 11. Comparison of field dependence of critical current density at 77 K, for conventional solid-state-sintered YBCO, melt-textured YBCO, and the epitaxial YBCO thin films. The figure shows improvement in J_c as a function of processing. Courtesy of 14 and 15.

in this area, with the main conclusion that the broken line curve in Fig. 16 displays the T_c (x) variation separating the superconducting phase $(x < x_c)$ from the antiferromagnetic insulators $(x > x_c)$ near $x = x_c = 0.13$ (36). This is the typical result for samples prepared by standard solid-state reaction at ambient pressure of oxygen (henceforth referred to as APO). Recently, it has been demonstrated that the underlying phase diagram is actually an artifact of sample processing. When these samples undergo an additional sinter at 915°C at elevated pressures of oxygen (220 atm of pure oxygen),T_c (x) increases qualitatively, and all the samples studied up to $x = 1/3$ are rendered superconducting with a T_c greater than 50 K. In particular, samples that were considered to be antiferromagnetic insulators $(x > 0.13)$ have been rendered superconducting, thus altering the presently accepted superconducting-antiferromagnetic phase diagram. Powder X-ray diffraction measurements have shown that the average structure of the samples synthesized at high pressures of oxygen (henceforth referred to as *HPO*) are also tetragonal as the usual samples synthesized at APO, except for a small excess of oxygen. The Fe local environments as revealed directly in Mössbauer spectroscopy measurements in the two types of samples (*APO* and *HPO*) at the same value of x are, however, qualitatively different, suggesting that aspects of dopant-centered local structures control in a remarkable way the superconducting behavior in these cuprates. There are plausible reasons to suggest that the majority of Fe resides in the CuO_3 chains, but that in APO samples at least Fe^{3+} does not replace Cu^{2+} but instead acquires a tetrahedral co-ordination as exemplified by Ga^{3+} cations in $Y_1Sr_2Ga_1Cu_2O_7$ superconductors (37). In HPO samples,Fe^{3+} is oxidized to Fe^{4+} with localization of an additional oxygen atom in its near-neighbor coordination, thus qualitatively changing the local site symmetry. The Co doping effects in YBCO bear a similarity to those of Fe doping, although the effects are less dramatic. The HPO sintering of APO samples increases the T_c quantitatively in general at doping concentrations $x < x_c = 0.20$. At $x > x_c$, antiferromagnetism sets in, and even HPO synthesis is unable to transform such samples to superconductors. The Ni doping effects in YBCO are apparently unaffected by

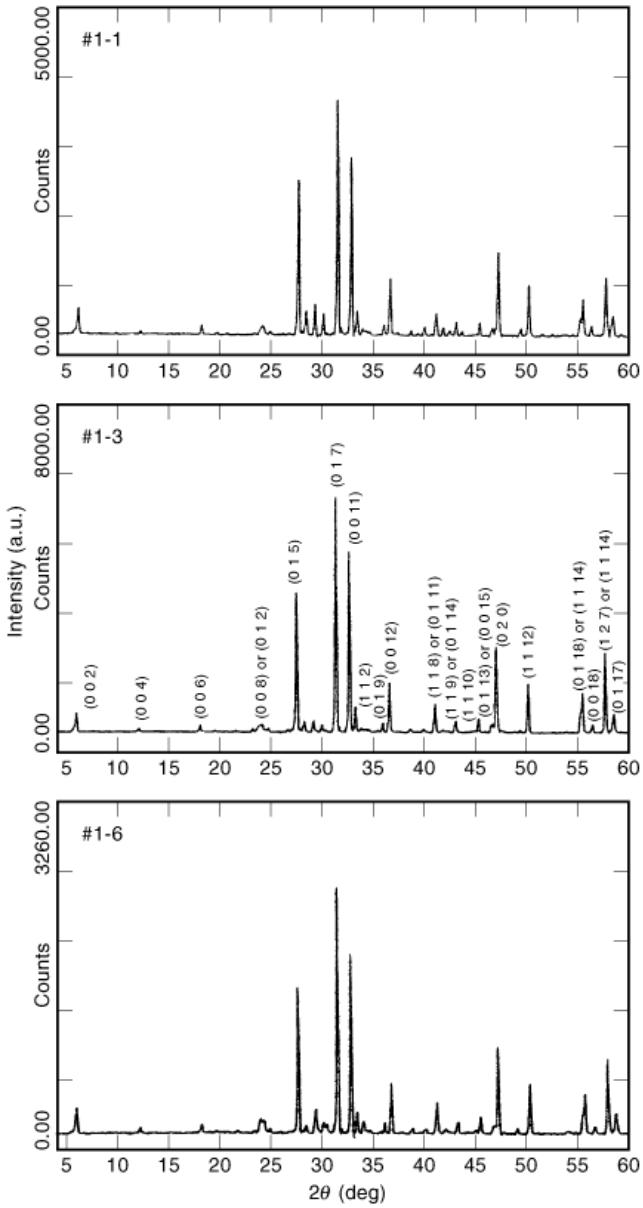

Fig. 12. Powder X-ray diffraction spectra obtained three Tl2212-sintered samples processed at different conditions as outlined in the text.

HPO synthesis as revealed by the results shown in Fig. 16. The T_c (x) variation of Ni-doped YBCO samples sintered at APO is similar to the variation in HPO samples. In contrast to Fe and Co doping, Ni doping in YBCO does not alter the lattice symmetry, which remains orthorhombic, probably because the dopant enters the structure substitutionally as Ni^{2+} replacing Cu^{2+}. The Fe and Co dopants enter the structure in higher charge states Fe^{3+} and Fe^{4+}, Co^{2+} and Co^{3+} largely in planes and bring in additional oxygen to alter not only the

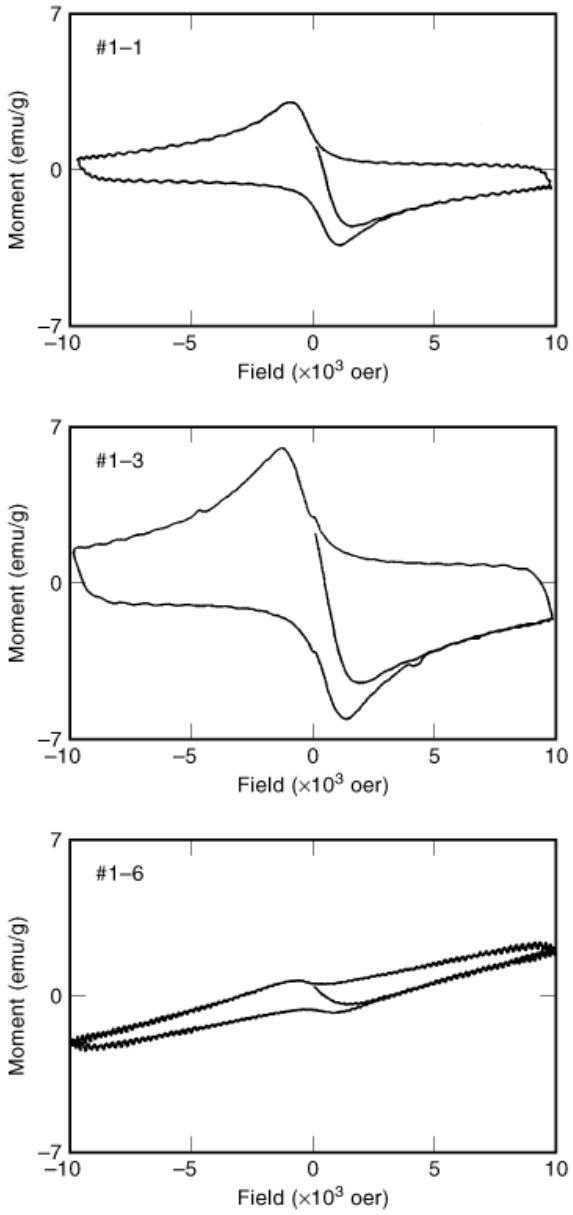

Fig. 13. Diamagnetic response of the samples 1.1, 1.3, and 1.6 obtained using VSM at 15 K. Sample 1.3 shows the largest diamagnetic susceptibility among the three samples, indicating that the heat treatment procedure used for sample 1.3 is close to the optimum.

lattice symmetry, which changes from orthorhombic to tetragonal, but also to create new local structures. The nature of these local structures continues to be a subject of current interest in large part because there appears to be a close correlation between the existence of specific structures and appearance of bulk superconductivity. These new results also demonstrate that Fedoped YBCO samples synthesized at HPO are chemically more

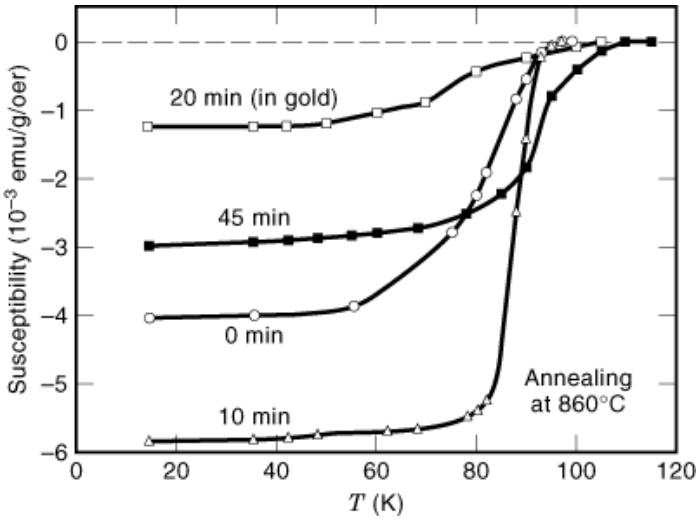

Fig. 14. The temperature dependence of magnetic susceptibility obtained from VSM measurements. Sample 1.3 shows the sharpest transition among the samples studied.

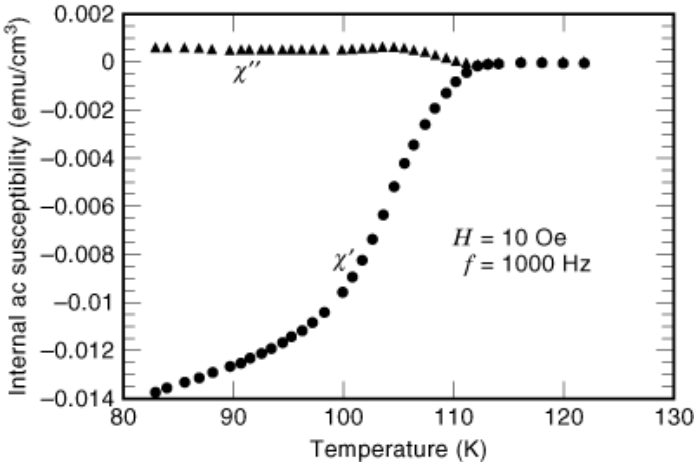

Fig. 15. The ac susceptibility measurement of a 1223 sample with $x = 0.75$ obtained using an ac susceptometer.

stable that those synthesized at APO. The higher chemical stability of HPO-synthesized YBCO samples may be attractive for various applications of bulk, thin films, and wires.

Processing of Hts Thin Films

***In-Situ* Versus *Ex-Situ* Processing.** Thin films of HTS materials (see THIN FILMS) have been deposited on a wide variety of substrates using two different procedures: *in-situ* processing and *ex-situ* processing. Both processes require high-vacuum deposition systems. *In-situ* processing is a technique in which the samples are deposited and processed inside a vacuum chamber and may not require any postprocessing outside the

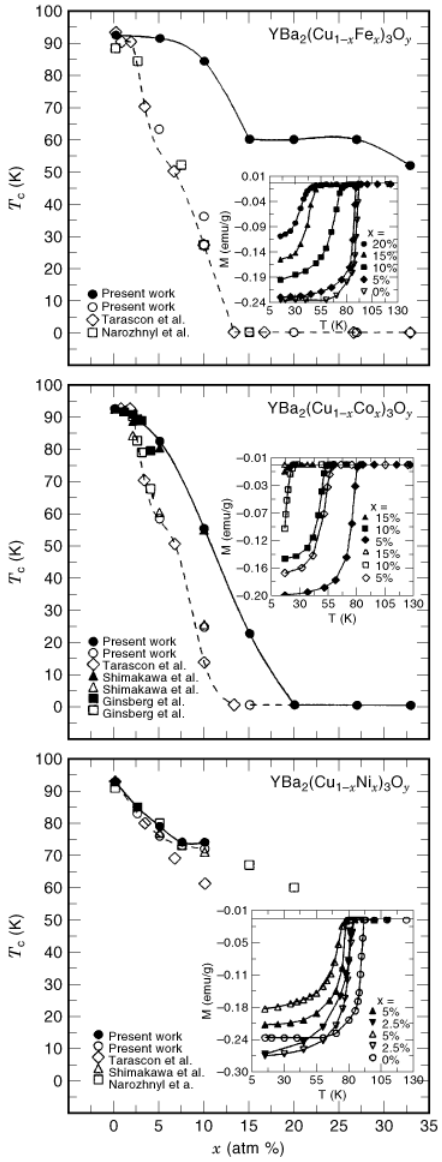

Fig. 16. T_c plotted as a function of metal doping concentration x for M = Fe (top panel),M = Co (middle panel) and M = Ni (bottom panel) in YBCO samples synthesized a high P (filled symbols) and at ambient P (open symbols). Lines drawn through data points are guides to the eye. The T_c values determined either magnetically or resistively are representative of a vast literature. Magnetization measured in a 20 G field, in the zero field cooling mode, are displayed in insets.

chamber (i.e., the samples they will be superconductors when they are removed from the vacuum chamber). The *ex-situ* processing method, on the other hand, requires postprocessing of samples outside the chamber. A deposition process will yield an amorphous material if the substrates are not heated; therefore, additional heat-treatment becomes necessary to obtain superconducting samples. The *In-situ* procedure is preferred because it leads to thin films with uniformity, with good control over the growth process and stoichiometry.

An *in-situ* deposition process usually uses a complex deposition system configured with a substrate heater assembly and process-monitoring capabilities. *in-situ* processing allows growth of multilayers with precise thickness control, essential for applications such as coated thin film conductors on metallic substrates with buffer layers. A drawback of the method is that it is not suitable for deposition on large area substrates. An *ex-situ* procedure is a simpler process because it is easier to optimize, and one can obtain reasonably good quality HTS thin films with postprocessing outside the vacuum chamber. The system requirements are less expensive compared to *in-situ* processing and are possibly applicable for thick or coated films of superconductors.

Physical and Chemical Deposition Methods. Deposition of HTS thin films can be done using either a physical or a chemical deposition method. The physical deposition methods include techniques such as sputtering, electron beam evaporation, and pulsed laser ablation or deposition. Chemical deposition methods include techniques such as metal-organic chemical vapor deposition (*MOCVD*) and metal-organic decomposition (*MOD*) (see THIN FILMS). Primarily, physical deposition techniques include some form of high-energy ion or electron bombardment of the target to release the material for deposition onto substrates. A chemical deposition method involves chemical vapors (transported using a gas such as hydrogen or nitrogen) reacting at the surface of heated substrates to form a thin film of desired composition. Both physical and chemical methods can be tailored for *in-situ* or *ex-situ* processing. Among the deposition methods, sputtering and pulsed laser deposition (*PLD*) are the most popular methods used, especially for the *in-situ* processes (see THIN FILMS).

Pulsed Laser Deposition. Pulsed laser deposition has been successfully used to deposit HTS thin films for *in-situ* processing; PLD is designed to replicate target stoichiometry in the deposited thin films (38). A typical PLD system consists of an ultra high vacuum chamber containing fused quartz windows for *in-situ* spectroscopic investigations. Pulsed laser deposition is a vapor phase deposition process in which a focused pulsed laser beam of energy density (also called fluence) exceeding 1 J/cm^2 strikes a sintered composite target material at an angle of 45°, vaporizes the target, and grows a thin film on a heated substrate placed nearby. A CO_2 laser, a Nd:YAG laser, a XeCl, or a KrF excimer each have been successfully used for PLD growth of HTS. Multiple targets can be used with each target ablated for a required amount of time. In multitarget systems, a target is rotated and synchronized with an optical encoder for pulsing the laser. This helps reduce the focused laser beam's heating effects on the target. A water-cooled target holder is normally used for further heat removal. *in-situ* deposition of YBCO thin films is typically performed at an oxygen partial pressure in the 70 mTorr to 200 mTorr range, on substrates heated in the range of 600° to 800°C depending on the choice of substrates. The presence of oxygen is required for compositional control of the oxide superconductors. After deposition, an oxygen anneal of the deposited film is performed for several hours at a reduced temperature (400° to 500°C), with slow cooling, in a higher oxygen partial pressure of 500 mTorr to 700 mTorr to obtain superconductivity (38,39).

Typical growth rates using a PLD system are in the range of a few angstroms per second. The growth parameters controlling the quality of thin films include the choice of the substrate, substrate temperature, background pressure of the vacuum system, laser energy density, frequency of the laser pulse sequencer, and oxygen partial pressure in the system. The HTS thin films prepared by PLD have excellent surface morphology, although one of the problems encountered has been the presence of particulates on the surface of such thin films. Understanding the chemistry of the laser interaction with emitted radicals of the target material is essential to control the growth quality of thin films over large areas and continues to be a subject of current research.

Sputtering of Thin Films. Sputtering is perhaps one of the more popular deposition methods used in the semiconductor industry for metals and dielectric materials. Broadly, there are two methods used: dc sputtering and RF sputtering. Both methods use ion plasma, typically argon, because of its inertness. High-energy ions bombard a target material to release target atoms, which are deposited on a substrate. Substrates can be heated to a high temperature for *in-situ* processing of materials. A modified method in sputtering, called magnetron sputtering, uses a magnetic field at the target to confine the plasma, which leads to higher deposition rates at low working gas pressures. Sputtering systems can employ either a single target or multiple targets. A

multitarget sputtering system gives precise control in multilayer depositions, because one can deposit a chosen target for a desired time, close a shutter and move on to the next target, essential for deposition of multilayers. Single-target systems are inexpensive and easier to use. Due to differing sputtering rates of various atoms, control of their relation content in a thin-film is difficult. In general, sputtering is susceptible to effects such as negative ion bombardment, which are primarily due to oxygen ions bombarding and resputtering the deposited thin film. One way to minimize negative ion bombardment is to use an off-axis geometry in which a substrate is mounted transverse to the target assembly. Process optimization is difficult to achieve for deposition of complex oxides such as the HTS materials. Some of the process parameters that need to be optimized include the target stoichiometry, partial pressure of the inert gas, RF or dc power density, substrate-target distance, and the substrate temperature. High-quality YBCO, TBCCO, and TPSCCO superconducting thin films and multilayers have been deposited using off-axis magnetron sputtering (40,41).

Metal-Organic Chemical Vapor Deposition. Metal-organic chemical vapor deposition is a proven technique for deposition of high-quality compound semiconductors. In principle, the advantages of MOCVD are the ease of large-area depositions, with high deposition rates and without a need for sophisticated high vacuum systems. However, the control of precise composition of the precursors is very difficult, and only small area films have been made to date. The MOCVD uses a deposition technique in which the required atomic constituents are transported in the form of vapors of metal-organic precursors by an inert transport gas such as argon or nitrogen, premixed with an oxidizing gas. Metal-organic precursors are placed in stainless-steel containers and heated to temperatures between 200° to 500°C to release vapors of the metal-organics. These vapors react with the heated substrate inside a reaction chamber. Mass flow controllers are used to control flow rates for each precursor. Mass flow rate, oxygen partial pressure and temperature of the substrate are some of the important process parameters. Typical metal-organic precursors for YBCO include metal β-diketonates such as $Y(C_{11}H_{19}O_2)_3$, $Ba(C_{11}H_{19}O_2)_3$, and $Cu(C_{11}H_{19}O_2)_3$ (42). A modification of this deposition technique is also currently used and is called the metal-organic decomposition (43). In this technique, metal carboxylates or acetates dissolved in an organic solvent are spin-coated on a substrate. The coated material is heat-treated at high temperatures to obtain the desired HTS phase. The technique is simpler to use because it does not require high vacuum equipment and is easily scalable for large area samples. The MOD does show promise for long-length wires. However, it is not pursued by many researchers due to the difficulty of producing films with only *c*-axis-oriented grains.

In our study, we have deposited *in-situ* films of YBCO on MgO substrates using the off-axis RF magnetron sputtering (18) process. Typical sputtering conditions for YBCO thin films are substrate temperature of 700°C, sputtering gas pressure of 500 mTorr, oxygen partial pressure of 10 mTorr, RF power of 60 W, and a target dc bias of −30 V. We have also processed Tl2212 thin films by on axis RF magnetron sputtering, and *ex-situ* processing. Tl2212 films were fabricated from both Tl2212- and Tl2223-sintered superconducting compounds at an RF power of 220 W, chamber pressure of 5 mTorr. Such thin films had to be postprocessed in an excess Tl_2O partial pressure, provided in the form of sintered 2223 pellets in a platinum crucible used for sintering. In both cases, heat treatment times and temperatures were optimized to obtain smooth morphology, high phase purity, and superior electrical and microwave properties (44).

Sputtering of TlCaBaCuO thin films from a sintered powder target was performed using pure argon gas. The reason for not using oxygen and reactive sputtering is the volatility of Tl from the target. Tl readily combines with oxygen and forms Tl_2O_3 which can be easily pumped out from the chamber. The target gets depleted of Tl much faster when oxygen is used as part of the reactive gases. The sputter-deposited thin films were postprocessed in two steps: first, sintering in air at 850°C for 12 min to 15 min in an excess Tl_2O partial pressure and, second, annealing in an oxygen flow of 500 sccm at 750°C for 15 min to 30 min. An excess Tl partial pressure was maintained during the annealing process. Sintering was performed in a small box furnace in the free surface configuration (45). Thin films were placed on a sintered pellet of Tl2223 with the film side facing the free surface in a small covered platinum crucible. A second pellet was placed above the sample in a platinum wire mesh support. The pellets provided the excess Tl partial pressure in the crucible to minimize the

loss of Tl from the thin film. Sintering of TlCaBaCuO thin film at 850°C in air for 12 min to 15 min established the superconducting phase and morphology. At 850°C, Tl_2O_3 decomposes into a liquid Tl_2O phase, which rapidly sinters with other constituents. After sintering, the crucible was removed from the furnace and cooled rapidly. Oxygen annealing of the air-sintered TlCaBaCuO thin film was carried out in the same configuration as used for sintering, with an oxygen flow of 500 sccm to 1000 sccm. During oxygen annealing, thin-film grains grow into large platelets. Oxygen annealing thus improves the electrical properties of the thin film by increasing its oxygen content.

Another promising method for the growth of high-quality Tl-based HTS thin films is called the Tl_2O_3 vapor process or the thallination process (46). In this process, thin films of the precursor materials of BaCaCuO or SrCaCuO are deposited using any of the thin-film deposition methods, and then the samples are heat-treated in a Tl_2O_3 vapor pressure. Tl_2O_3 vapor diffuses into the precursor and reacts to form the superconducting phases in the films. This technique is safer because the vacuum deposition chamber is not contaminated with the Tl_2O_3 vapors.

Characterization of Processed Superconducting Thin Films. The XRD provides one of the direct characterizations of grown thin films because it gives information on the phase purity, their lattice constants, and their crystallographic orientation with respect to the film plane. Electrical transport measurements are performed for accurate measurement of transport current density at zero field as well as at finite magnetic fields. The transport current measurements involve patterning a four-probe test structure on the HTS films. The four-probe test devices are designed with line widths of 10 μm to 1 mm depending on the nature of the measurements.

The geometry of a typical test device is shown in Fig. 17. The test structure consists of two outer pads through which a constant current source is applied and a voltage is measured across the voltage sensing lines, which are 1 mm apart. The width of the voltage sensing should be less than the width of the line connecting pads 1 and 2 in order to approximate a point contact as closely as possible. The test devices are patterned on superconducting thin films using standard positive photoresist photolithography and a wet chemical etching technique using a 1:100 phosphoric acid:DI water solution. A pulsed current is applied between the outer pads, and the voltage across the outer sense lines is monitored. The electric field criterion of 1 μV/cm is typically used (i.e., the current through the sample at which measurement of 1 μV potential difference over a 1 cm spacing develops gives an estimate of the superconductor's critical current). Also, the same test structure can be used to determine the T_c from temperature (T) dependence of resistivity (47). In such a measurement, a constant dc current of 10 μA is applied through the outer terminals, and the voltage across the sense lines is related to the resistance of the sample. Knowing the exact thickness of the superconducting thin film and the cross-section, the T dependence of resistivity plot can be obtained.

Structural, Electrical, and Magnetic Properties of Thin Films. High-quality YBCO and Tl2212 HTS thin films have been grown on various substrates such as YSZ, $LaAlO_3$ (LAO), $SrTiO_3$ (STO), CeO_2, and MgO. Figure 18 shows an XRD scan of an annealed Tl2212 thin film on LAO substrate. The figure shows characteristic reflections of Tl2212, Tl2223 phases as well as those of the LAO substrate. From the prominent (0 0 l) reflections observed in the XRD spectrum, the highly c-axis-oriented growth is evident. The Tl2212 phase is the dominant one in the film, as determined from the intensities of the XRD peaks. The c-axis lattice constant calculated from the XRD scan is found to be 29.2 Å. The a-axis lattice constant of $LaAlO_3$ is 3.7801 Å. The a-axis lattice constant of Tl2212 phase is 3.8503 Å. Thus, the lattice mismatch is less than 2%.

Figure 19 shows the temperature dependence of resistivity for one of the Tl2212 thin films deposited on LAO, using a 50 μm wide four-probe device with zero applied magnetic field. The zero-resistance T_c is approximately 100 K for the thin film. Figure 20 shows the typical zero field J_c variation with temperature obtained using a four-probe test device.J_c Values at zero magnetic field as high as 5×10^5 A/cm^2 at 77 K and approximately 1×10^6 A/cm^2 at 60 K were obtained. The surface morphology of the films was essentially featureless and smooth, which is typical of high-quality films. In general, the J_c of Tl2212 and Tl1223 thin films are lower than the J_c of epitaxial YBCO thin films. The presence of grain boundary weak links and

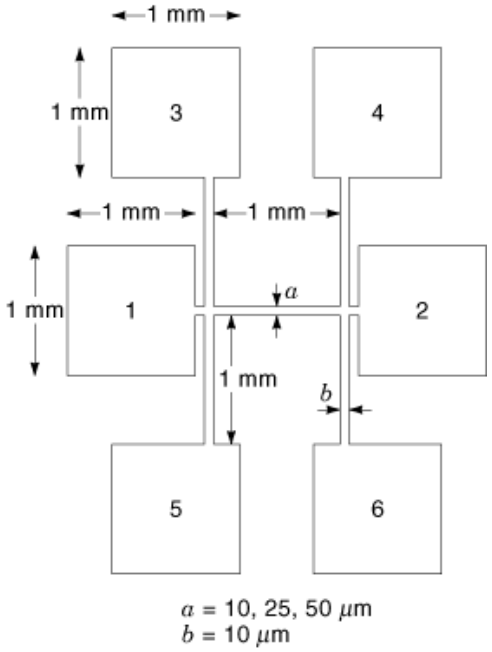

Fig. 17. Geometry of four-probe test devices used for electrical transport measurements. A current source is connected between pads 1 and 2, and corresponding voltage measurements are taken across either pads 3 and 4 or pads 5 and 6.

weak flux pinning in thallate thin films may be the main reasons for the lower J_c compared to epitaxial *in-situ*-grown YBaCuO thin films. However, among the polycrystalline HTS, Tl2212 and Tl1223 thin films have shown superior electrical properties; hence, such films are very attractive for electronic applications (48). *in-situ* processing of Tl2212 and TlPb1223 superconducting thin films has not been highly successful owing to the complex chemistry of the thallic oxides. Tl2212 and Tl1223 thin films with very low surface resistance (at least two orders of magnitude below the oxygen-free copper conductor) at frequencies as high as 12 GHz and a current density greater than 10^6 A/cm^2 are routinely obtained (48).

Processing of Superconducting Wires and Tapes

HTS Wires and Tapes, First Generation. The Bi2223 compound is perhaps the more attractive compound for processing conductors because its T_c (110 K) is higher than that of the Bi2212 compound (90 K). Surprisingly, the Bi2212 compound has better magnetic field dependence of J_c at 4 K, primarily due to better electromagnetic connectivity. At 77 K, the Bi2223 phase clearly has higher J_cs compared to the Bi2212 phase. The best BSCCO HTS conductors have J_cs KA/cm^2 as high as 20 to 70 kA/cm^2 at zero field with J_c also depending on the length of the conductor (49). Oxide powder-in-tube (*OPIT*) has been a widely used technique for processing long lengths of BSCCO wires.

OPIT Method for BSCCO 2212 and 2223 Superconducting Wires. Lead (Pb)-doped Bi2223 and Bi2212 are prime candidates for OPIT synthesis of long-length HTS wires. Of these two phases, Bi2212 is easier to synthesize. The reaction kinetics and thermodynamics for synthesis of the pure Bi2223 phase are quite complex and generally result in mixed phase samples, with the presence of Bi2223, Bi2212, and other secondary phases. Partial substitution of lead for bismuth is generally found to stabilize growth of the Bi2223

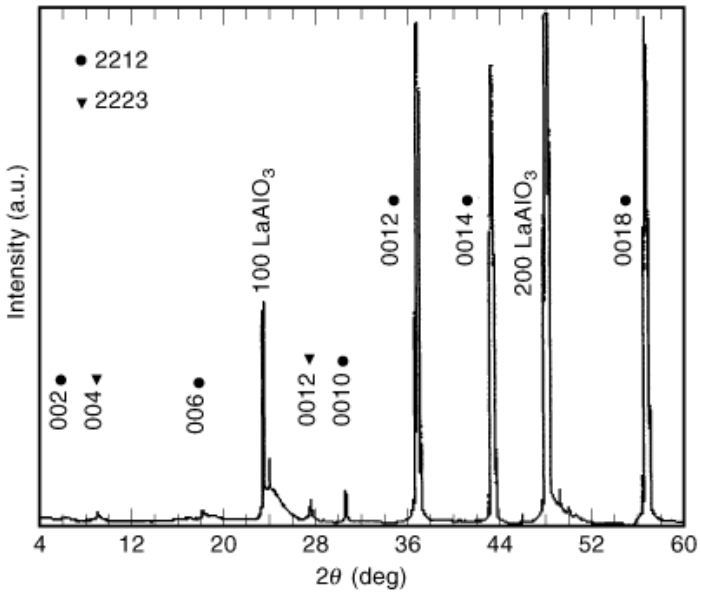

Fig. 18. XRD reflections observed on a Tl2212 thin film on a LAO substrate. The reflections correspond to the Tl2212 phase, the Tl2223 phase, and the substrate.

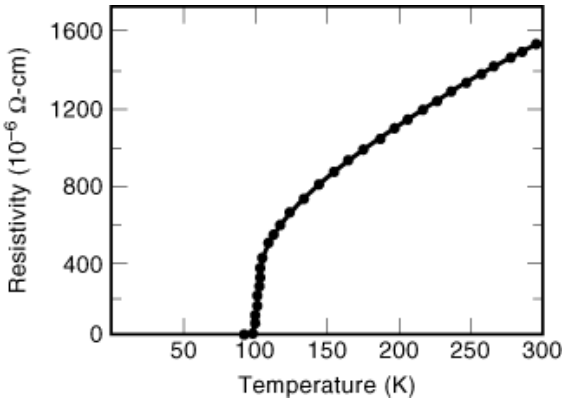

Fig. 19. Temperature dependence of electrical resistivity for a 50 μm wide Tl2212 thin film four-probe test device.

phase with a typical starting composition of Bi:Pb:Ca:Sr:Cu given by 1.8:0.4:2:2:3 for such growth (50). Figure 21 pictorially shows the four steps involved for the OPIT method of preparing HTS wires and tapes. In step 1, the precursor powder is prepared from a solid-state reaction (or calcination) of mixtures of Bi-, Cu-, and Pb- oxides and Sr- and Ca- carbonates in an alumina crucible at temperatures between 800° and 860°C for 48 to 60 h in air. Another approach for synthesis of the precursor material is to mechanically alloy the chemicals for higher packing density. In step 2, the precursor powder is filled inside a silver billet and then drawn into fine filaments less than 1 mm in diameter. Several tens to a hundred of these filaments are stacked in a silver tube, drawn, and then rolled into tapes 4 mm to 6 mm wide, and typically 0.2 mm thick in step 3. Finally, in step 4, OPIT tapes are processed in the presence of a partial melt, which aids in densification and

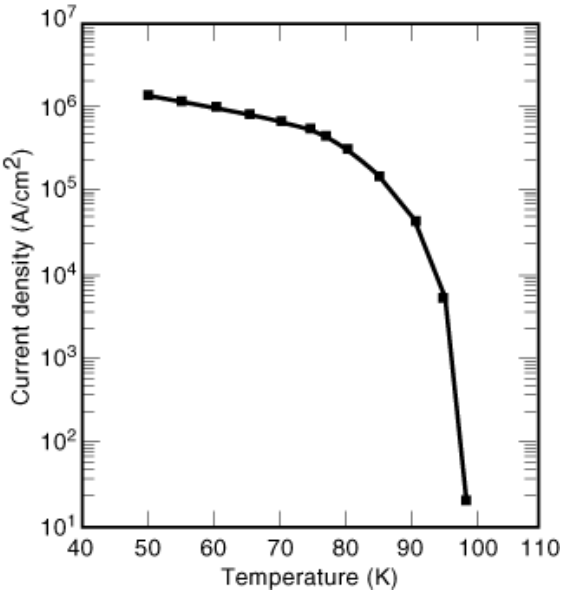

Fig. 20. Typical temperature dependence of zero field current density for a postprocessed Tl2212 thin film. Measurements were performed on the four-probe test devices.

grain growth. To create a partial melt, the sample is heated above 900°C for a short time, followed by a long anneal of approximately 100 h at 840 to 850°C. At present, such tapes can be reliably manufactured in several kilometer scale lengths. The main process parameters involved in the synthesis of wires thus include precursor material synthesis, mechanical processing, and heat treatment conditions. The precursor composition, particle size, and density are important factors in the quality of precursor material synthesis (51). Billet dimensions, filament restacking geometry, and mechanical properties of the tape are the important mechanical aspects for wires and tapes of HTS. Heating rate, sintering temperature, sintering time, and cooling rate are important parameters for heat treatment conditions that control electrical and mechanical properties of drawn wires. Heat treatment is performed after cutting wires to required lengths. Each filament is embedded in a silver matrix, which adds mechanical strength and flexibility. A threshold value for silver content is required to enhance electromagnetic grain connectivity, essential for long length conductors. At the same time, one needs to maximize the superconducting volume fraction so that the HTS rather than the silver present in the conductor provides the percolative path for charge carriers. Fill factor is one of the critical parameters in HTS wires, defined as the ratio of the volume of the superconductor core to the entire volume of the conductor. Typical fill factor in most HTS conductors to date is below 60% (51). Magneto-optic studies indicate that most of the current transport occurs at the interfacial region between silver and the bulk BSCCO rather than in the bulk BSCCO (52). The interfacial region with well-aligned grain structure appears to be the key to improve J_cs in these wires. The Bi2212 phase is attractive for low-temperature applications at 4 K because it is economical to produce long length multifilamentary conductors (52).

HTS Wires and Tapes: Second Generation, YBCO-Coated Conductors. Primarily because of the higher J_cs demonstrated in biaxially textured thin films;. YBCO has enormous advantage over BSCCO for wire applications. One approach is to grow YBCO on a biaxially textured chemically compatible buffer layer. A processing technique proposed for biaxial texturing of chemically compatible buffer layers on untextured substrates such as alloys of nickel is called the ion-beam-assisted deposition (*IBAD*) (53). Another approach proposed is the biaxial texturing of the substrates. It is well known that metals when deformed into wires

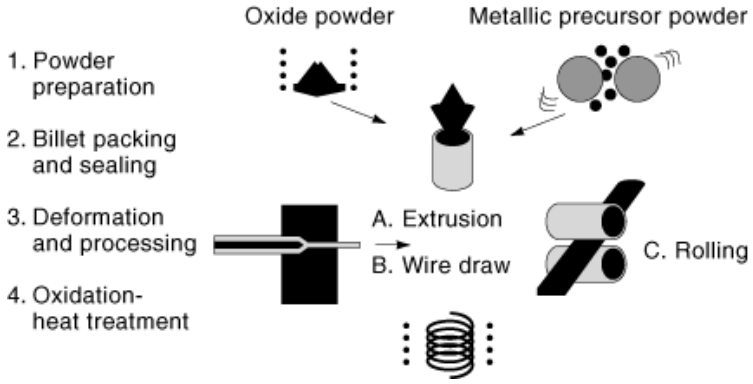

Fig. 21. Schematic diagram showing the general OPIT process used to produce BSCCO tapes, developed by American Superconductor Corporation. Courtesy of 15.

develop alignment along preferred directions. Recent work at Oak Ridge National Laboratory has shown that biaxially textured [i.e., both in-plane and out-of plane alignments (ab)] nickel can be produced over long lengths (54). Such substrates are called rolling assisted biaxially textured substrates (*RABiTS*) (54). An interesting example of biaxial texturing of metallic sheets already used in electrical engineering is in silicon-doped steel stampings used in the electric power industry, in which texturing results in the easy direction of magnetization parallel to the length of sheets, reducing hysteresis losses.

The IBAD process is used primarily for deposition of buffer layers such as yttrium-stabilized zirconia (*YSZ*), or cerium oxide (CeO_2) on untextured nickel alloy tapes (53). The IBAD process is a thin-film deposition process developed by IBM for preferential growth of biaxially textured buffer layer material on untextured substrates. In this process, a rare gas ion beam is used to bombard the buffer layer along a preferred crystallographic direction as it is being deposited. The angle of incidence of the ion beam with respect to the plane of the substrate is the critical parameter for the preferential orientation of the buffer layer grown. Typical buffer layer of choice for IBAD has been YSZ, grown to a thickness of 200 nm to 500 nm. A thin layer of CeO_2 is interposed between YSZ and YBCO for better lattice matching. Subsequent growth of postprocessed YBCO thin or thick films on the biaxially oriented buffer layers have yielded high J_cs $> 10^5$ A/cm^2 at 75 K and in magnetic fields up to 5 T. Figure 22 shows the J_c versus magnetic field characteristics obtained for a short sample of a 1.6 μm thick YBCO/IBAD-YSZ/Ni alloy tape, at 75 K (53). The figure also shows the magnetic field dependence of J_c for a proton-irradiated Bi-2223 OPIT wire for comparison. The figure clearly shows the vastly improved performance of the IBAD tape compared to the best OPIT wire. An advantage of the IBAD-buffered HTS tapes compared to OPIT wires is that the tapes can be wound with the HTS in compression, attractive for electromagnetic applications such as electric motors, and generators. Current efforts are underway to scale-up the process for long lengths necessary for commercialization.

The Rolling assisted biaxially textured substrates (*RABiTS*) process was developed by Oak Ridge National Laboratory for epitaxial growth of HTS thin films over long lengths. Figure 23 schematically shows the process for the development of *RABiTS* (54). Nickel is the primary candidate for the *RABiTS* because of its higher oxidation resistance compared with copper. Also, thermomechanical texturing of Ni gives a cube-textured substrate. A typical YBCO thin-film-coated conductor fabrication process involves thermomechanical processing of Ni substrate (125 μm), followed by PLD of buffer layers of CeO_2 (0.2 μm), YSZ (0.2 μm), and finally 1 μm thick YBCO film PLD deposited at $\sim$780°C in an oxygen pressure of 185 mTorr (54). After deposition, the film is cooled at 10°C per min, in an oxygen pressure of 700 mTorr at 400°C. All oxide buffer layers are grown at temperatures of 780°C. *RABiTS* of lengths up to 100 feet (only the substrates with no HTS) have been processed

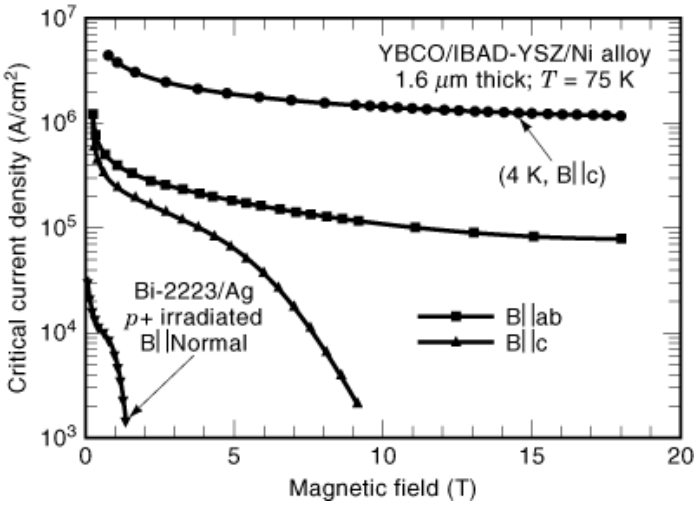

Fig. 22. J_c versus applied magnetic field for a 1.6 μm IBAD tape as a function of magnitude and orientation with respect to the tape plane, compared with a proton-irradiated OPIT BSCCO 2223 wire. Courtesy of 14.

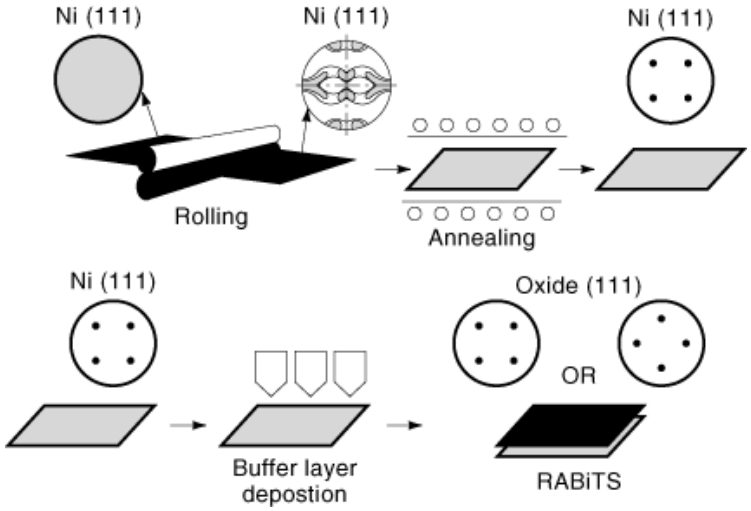

Fig. 23. Schematic representation of the *RABiTS* process developed at Oak Ridge National Laboratory. Starting with a randomly oriented Ni bar/plate, cold rolling is used to produce a distinct copper-type rolling texture. This is followed by recrystallization to a cubic structure. Epitaxial metal and/or oxide buffer layer(s) are then deposited on the textured Ni. Courtesy of 54.

already.J_c values of a short YBCO thin-film-coated conductor are shown in Fig. 24. For comparison, thin films of YBCO on LAO and thin films of Tl2212 and 1223 on LAO are also shown. Because PLD and sputtering techniques are not scalable, MOCVD may be the primary technique for long-length HTS-coated conductors on *RABiTS*. The MOCVD-grown YBCO on *RABiTS* has yielded zero field J_c as high as 0.64 MA/cm^2 at 77 K.

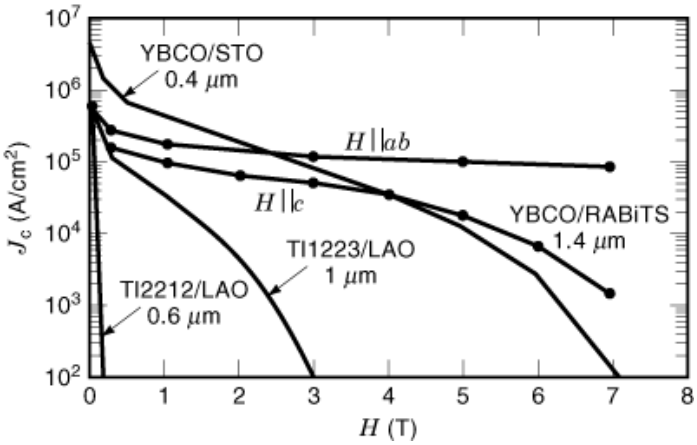

Fig. 24. The critical current density versus magnetic field for YBCO thin film on a *RABiTS* substrate of configuration ML3 corresponding to YSZ(110) (0.5 μm)‖Ni(100) (125 μm). Data for both $H\|c$ and $H\|ab$ are shown. Also shown are data for YBCO thin film on STO, Tl2212, and Tl1223 thin films on LAO substrates. For $H\|c$, the high-field properties of YBCO thin films on *RABiTS* are better than those on STO. Courtesy of 54.

Applications of High-Temperature Superconductors

Bulk superconductors can be used in applications such as high Q cavities for microwave applications see Superconducting microwave technology, frictionless bearings, magnetic levitation (see Superconducting levitation), and fault current limiters (see Superconducting fault current limiters). Melt-textured as well as single crystal bulk YBCO conductors have been used as a microwave cavity with very high Q values greater than 10,000 at 77 K and at frequencies below 20 GHz. Progress in bulk single-crystal growth could be attributed to newer crucible materials such as $BaZrO_3$ (55). The use of $BaZrO_3$ crucible precludes impurities such as Al, Zr in melts or crystals for the growth of 123 rare-earth-based HTS.

Thin film HTSs are most attractive for microwave applications because of their low surface resistance at frequencies upto 35 GHz (see Superconducting microwave technology and Superconducting filters and passive components). A large number of microwave components have been demonstrated using HTS technology, (e.g., high Q filters resonators, phase shifters, delay lines). Epitaxial growth of HTS thin films on low-loss microwave substrates such as MgO and sapphire (with a CeO_2 buffer layer) has been key for high Q microwave components. A promising new application in this area involves integration of HTS thin films and ferroelectric thin films for electrically tunable components (56). Tunable filters, resonators, and phase shifters have been successfully demonstrated. We have recently reported a two-pole tunable bandpass filter using a thin-film YBCO/STO/LAO multilayer microstrip configuration. The structure consists of a LAO substrate (254 μm thick) on which an epitaxial STO thin film (0.3 μm thick) was deposited by PLD, followed by a YBCO thin film (0.35 μm thick) deposited by PLD. The two-pole filters were designed for a center frequency of 19 GHz and 4% bandwidth. Tunability is achieved through the nonlinear dc electric field dependence of relative dielectric constant of STO thin films. Figure 25 shows the swept frequency response of a tunable filter at 77 K, for bipolar bias voltages between 0 and $\pm$500 V (56). Note that the insertion and return losses are reduced with applied bias. Although high voltages are required, the power consumption is low owing to negligible currents through the high dielectric constant ferroelectric thin film.

Another area of electronics in which HTS thin films have a niche is in the use of HTS SQUIDs (see SQUIDS) as magnetic field sensors. A SQUID operates on the principle that the critical current through two Josephson junctions connected in a loop is a function of the magnetic flux threading the loop. Since each SQUID

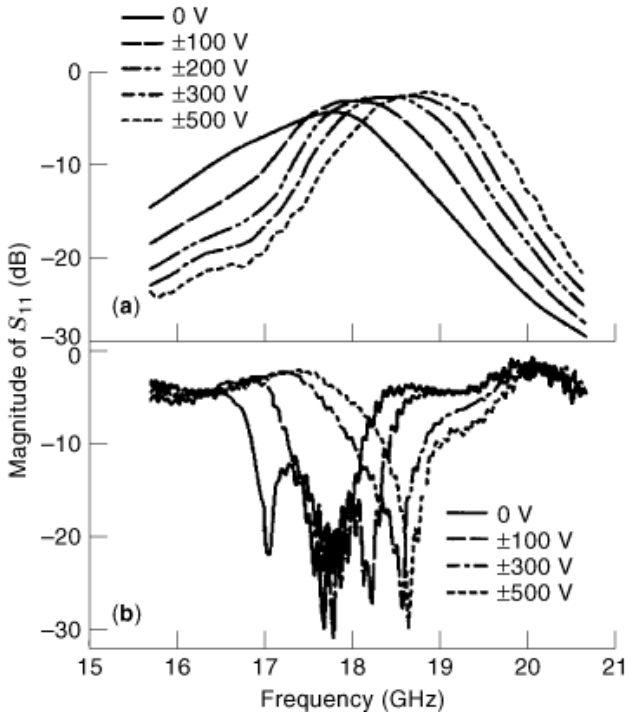

Fig. 25. Electric field tunability of a tunable bandpass filter using a thin film YBCO/STO/LAO multilayered microstrip structure. The filter uses the electric field dependence of the nonlinear dielectric constant of the STO ferroelectric thin film.

stores multiples of the basic flux quanta, SQUIDs are the most sensitive sensors of magnetic fields at levels of 10^{-14} T at 77 K, thus making possible measurements of magnetic fields produced by current flow in a human brain, about 10^{-13} T (see SQUIDS). The key to the HTS SQUID technology is the reproducible fabrication of grain boundary Josephson junctions. This technology has currently matured to the level of commercial usage in magnetic imaging for medical diagnostics such as a magnetoencephalography (MEG), mapping the brain's magnetic activity. Another area of application for HTS thin films is in interconnect technology for semiconductor multichip modules. With the promise of high-quality YBCO thin films on various buffer layers such as CeO_2, and YSZ, it is feasible to conceive of applications of HTS thin films on silicon substrates.

Applications such as nuclear magnetic resonance (*NMR*) require uniform magnetic fields over large volumes. Nuclear magnetic reasonance requires a field level of 10 T to 20 T. The NMR technique uses RF and magnetic fields to study transitions between nuclear spin states. An RF coil surrounds a sample, placed inside a magnetic field. The magnetic field is swept through a small range with a separate coil. A secondary RF coil (may be a superconducting coil) picks up the resonance signal. Use of superconducting coils in magnet technology has made possible high magnetic fields with minimal energy dissipation. Use of superconducting lines for power transmission is attractive for energy efficiency. The current densities needed for the utility power lines are considerably lower than most other power applications. It is estimated that current densities below 10^4 A/cm^2 at 77 K are sufficient for utility power lines. The Bi-based superconductors are the most attractive for these applications. The design of underground cables cooled to liquid nitrogen temperatures is a challenging aspect because these superconductors are detrimentally affected by moderate mechanical stresses. Superconducting magnetic energy storage (*SMES*) is an energy storage device wherein energy is stored in the magnetic field associated with circulating currents in superconductors. An SMES system consists of an ac/dc

Table 3. Companies Producing HTS Materials

American Superconductor Corporation
Two Technology Drive
Westborough, MA 01581
(508) 836-4200

Conductus, Inc.
969 W. Maude Avenue
Sunnyvale, CA 94086
(408) 523 9950

DuPont Superconductivity
Experimental Station E304/C110
Wilmington, DE 19880
(302) 695-9230

Intermagnetics General Corporation
PO Box 461, 450 Old Niskayuna Road
Latham, NY 12110-0461
(518) 782-1122

Superconductive Components, Inc.
1145 Chesapeake Avenue
Columbus, OH 43212
(614) 486-0261

Superconductor Technologies, Inc.
460 Ward Drive
Santa Barbara, CA 93111
(805) 683-7646

power converter to charge a large torroidal magnet. When needed, the energy stored in the magnetic field can be tapped and converted by ac power. Again HTS wires are needed for the large magnets used in such a system. Other applications attractive for HTS wires and tapes include power devices such as motors, generators and transformers. With the current technology, several prototypes of HTS wires and tapes have been demonstrated. American Superconductor Corporation had tested a 125 hp ac synchronous motor built using a BSCCO 2223 composite tape. A 5 kJ HTS SMES magnet, a high-current pancake coil (100 A), and current development of 500 and 1000 hp motors indicate that HTSs have potential for large-scale power applications (49). Table 3. shows some of the HTS companies which provide superconducting materials and fabrication services.

BIBLIOGRAPHY

1. W. Meissner R. Oschenfeld Ein Neuer Effekt bei Eintritt der Supraleitfahigkeit, *Naturwiss.*, **21**: 787, 1933.
2. F. London H. London The electromagnetic equations of the superconductor, *Proc. R. Soc. A*, **A149**: 71–88, 1935.
3. F. London *Superfluids, Macroscopic Theory of Superconductivity*, vol. **1** New York: Wiley, 1950, pp. 3-4.
4. J. Bardeen L. N. Cooper J. Schreiffer Theory of superconductivity, *Phys. Rev.*, **108** (5): 1175–1204, 1957.
5. B. D. Josephson Possible new effects in superconductive tunneling, *Phys. Lett.*, **1** (7): 251–253, 1962.
6. J. G. Bednorz K. A. Muller Possible HTS superconductivity in the Ba–La–Cu–O system, *Z. Phys. B*, **64**: 189–193, 1986.
7. M. K. Wu et. al. Superconductivity at 93 K in a new mixed phase Y-Ba-Cu-O compound system at ambient pressure, *Phys. Rev. Lett.*, **58** (9): 908–910, 1987.
8. H. Maeda *et al.* A new HTS oxide superconductor without a rare earth element, *Jpn. J. Appl. Phys.*, **27** (2): L209–210, 1988.
9. Z. Z. Sheng A. M. Hermann Bulk superconductivity at 120 K in the T1-Ca-Ba-Cu-O system, *Nature*, **332** (6160): 138–139, 1988.

10. S. N. Putilin *et al.* Superconductivity at 94K in HgBaCuO, *Nature*, London, **362**: 226, 1993.
11. J. D. Doss *Engineer's Guide to High Temperature Superconductivity*, New York: Wiley, 1989.
12. A. A. Abrikosiv On the magnetic properties of superconductors of the second group, *Soviet Phys. JETP*, **5**: 1174, 1957.
13. R. P. Huebener *et al.* Thermoelectric and thermomagnetic effects in high temperature superconductors, *Proc. Materials Res. Soc. Symp.*, 1992; pp. 13–22.
14. P. M. Grant Superconductivity and electric power: Promises, Promises ... Past, present, and future, *IEEE Trans. Appl. Supercond.*, **7**: 112–135, 1997.
15. T. P. Sheehan *Introduction to High Temperature Superconductivity*, New York: Plenum, 1994.
16. H. A. Blackstead J. D. Dow Implications of Abrikosov-Gorkov exchange scattering for theories of high temperature superconductivity, *Phys. Lett. A*, **206**: 107–110, 1996.
17. D. C. Larbalestier Road to conductors of high temperature superconductors: 10 years do make a difference!, *IEEE Trans. Appl. Supercond.*, **7**: 90–98, 1997.
18. C. Blue P. Boolchand *In-situ* preparation of superconducting YBCO 123 thin films by on-axis rf magnetron sputtering from a stoichiometric target, *Appl. Phys. Lett.*, **58**: 2036–2038, 1991.
19. S. Tanaka Reviews, prospects and concluding remarks. Materials needs for applications, *Physica C*, **282–287**: xxxi–xxxix, 1997.
20. M. A. Kirk H. W. Weber Electron microscopy investigations of irradiation defects in the high T_c superconductor YBCO, in *Studies of High Temperature Superconductors*, vol. **10** Commack, NY: Nova, 1992, p. 243.
21. S. Jin *et al.* Melt textured growth of polycrystalline YBCO with high transport J_c at 77K, *Phys. Rev. B*, **37**: 7850–7853, 1988.
22. S. S. P. Parkin *et al.* Bulk superconductivity at 125 K in $Tl_2Ca_2Ba_2Cu_3O_x$ *Phys. Rev. Lett.*, **60** (24): 2539–2542, 1988.
23. M. Greenblatt *et al.* Chemistry and superconductivity of thallium based cuprates, *Studies of the HTS Superconductors*, vol. **4** Commack, NY: Nova, 1992.
24. M. Murakami *et al.* Melt processing of bulk YBCO superconductors with high$_c$, *J. of Eng. Materials Tech.*, **114**: 189, 1992.
25. M. Murakami *et al.* Melt processing of bulk high T_c superconductors and their applications, *IEEE Trans. Magn.*, **27**: 1479, 1991.
26. V. R. Todt *et al.* Processing of large YBCO domains for levitation applications by a NdBaCuO seeded melt growth technique, *J. Electron. Materials*, **23**: 1127, 1994.
27. K. Salama S. Sathyamurthy Melt texturing of YBCO for high current applications, *Appl. Superconductivity*, **4** (10–11): 547–561, 1996.
28. Z. Sheng Tl-based high T_c superconductors, *Mater. Sci. Forum*, **130–132**: 1–34, 1993.
29. G. Subramanyam *et al.* Processing and physical properties of single phase TlBaCaCuO (2212) and (Tl-Pb) (Sr-Ba)CaCuO (1223) superconductors, *Appl. Superconductivity*, **4**: 591–598, 1996.
30. T. Kamo *et al. Appl. Phys. Lett.*, **59**: 3186–3188, 1991.
31. C. P. Bean Magnetization of high field superconductors, *Rev. Mod. Phys.*, **36**: 31–39, 1964.
32. W. M. Reiff Magnetic susceptibility measurements: An important facet of modern solid-state characterization, *Amer. Lab.* **26**: February 1994.
33. L. H. Greene B. G. Bagley Oxygen stoichiometric effects and related atomic substituitions in the high T_c cuprates, in *Physical Properties of High Temperature Superconductors*, vol. **II**, Singapore: World Scientific, 1990, pp. 509–569.
34. R. Sugise, *et al. Jpn. J. Appl. Phys.*, **27**: L2310, 1988.
35. B. Raveau *et al.* Layered thallium cuprates: Non-stoichiometry and superconductivity, *Solid State Ionic.* **39**: 49–62, 1990.
36. F. Shi *et al.* Metal (M) dopant centered local structures, high-pressure synthesis and bulk superconductivity in $YBa_2(Cu_{-x}M)_{3-}O_{7-\delta}$: M–Fe, Co, Ni, *J. Condens. Matter*, **9**: L307–L313, 1997.
37. A. Rykov V. Caignaart B. Raveau Quadrupole interactions and vibrational anisotropy of tetragonal Fe (111) in the 123 derivative $LnSrCuGa_{1-x}Fe_xO_{7-\delta}$ (Ln = Y, Ho), *J. Solid State Chem.*, **109**: 295, 1994.
38. J. Qiao C. Y. Yang High Tc superconductors on buffered silicon: Materials properties and device applications, *Materials Sci. Eng.* **R14**: 157–202, 1995.
39. D. C. Payne J. C. Bravman (eds.) Laser ablation for material synthesis, Materials Research Society (MRS) Fall Meeting, *MRS Symp. Proc.*, Vol. 191, Boston, 1990.

40. D. S. Ginley Thallium films for microelectronic applications, in A. M. Hermann, and Y. Yakhmi (ed.), *Thallium based superconducting Compounds*, Singapore: World Scientific, 1994.
41. W. Holstein *et al.* Superconducting epitaxial Tl2212 films on sapphire with cerium oxide buffer layers, *Appl. Phys. Lett.*, **61** (8): 982–984, 1992.
42. J. Zhao P. Norris Metalorganic chemical vapor deposition of YBCO 123 thin films, *Mater. Sci. Forum*, **130–132**: 233–254, 1993.
43. G. Braunstein *et al.* Process of formation and epitaxial alignment of $SrTiO_3$ thin films prepared by metal-organic decomposition, *J. Appl. Phys.*, **73**: 961–70, 1993.
44. G. Subramanyam *et al.* Studies on sputtered TlCaBaCuO high T_c superconducting thin films for microelectronics applications, *Materials Sci. Forum*, **130–132**: 613–632, 1993.
45. D. S. Ginley *et al.* Morphology control and high critical currents in superconducting thin films in the Tl-Ca-Ba-Cu-O system, *Physica C*, **160**: 42–48, 1989.
46. B. Johs *et al.* Preparation of high T_c Tl-Ba-Ca-Cu-O thin films by pulsed laser evaporation and Tl_2O_3 vapor processing, *Appl. Phys. Lett.*, **54**: 1810–1812, 1989.
47. W. Pelster Accurate automated measurement of superconductor material resistance, *Res. & Develop.*, **30**: 80–84, 1988.
48. DuPont Superconductivity, Technical Note on Tl based superconducting thin films, Wilmington, DE, 1998.
49. A. P. Malozemoff Q. Li. S. Fleshler Progress in BSCCO-2223 tape technology, *Physica C*, **282–287**: 424–427, 1997.
50. U. Balachandran *et al.* Processing and fabrication of high T_c superconductors for electric power applications, *Appl. Superconductivity*, **5** (1-6): 187–191, 1997.
51. V. Selvamanickam *et al.* High temperature superconductors for electric power and high energy physics, *J. Metals*, **50** (10): 27–30, 1998.
52. S. Brody The last days of BSCCO?, *Superconductor and Cryoelectronics*, featured article on BSCCO wires, **11**: 26–30, Spring 1998.
53. Y. Ijjima *et al.* In-plane aligned YBCO thin films deposited on polycrystalline metallic substrates, *Appl. Phys. Lett.*, **60**: 769–771, 1992.
54. A. Goyal *et al.* Epitaxial superconductors on rolling assisted biaxially textured substrates (*RABiTS*): A route towards high critical current density wire, *Appl. Superconductivity*, **4** (11–12): 403–427, 1996.
55. A. Erb E. Walker R. Flukiger The use of BaZrO3 crucibles in crystal growth of the high T_c superconductors: Progress in crystal growth as well as in sample quality, *Physica C*, **258**: 9–20, 1996.
56. F. A. Miranda *et al.* Tunable microwave components for Ku and K-band satellite communications, *Integrated Ferroelectrics*, **22**: 269–278, 1998.

GURU SUBRAMANYAM
University of Dayton
PUNIT BOOLCHAND
University of Cincinnati